Contrib Mineral Petrol (2006) 152: 149–167
DOI 10.1007/s00410-006-0098-z

ORIGINAL PAPER

Bernard W. Evans · Bruno Scaillet · Scott M. Kuehner

Experimental determination of coexisting iron–titanium oxides in the systems FeTiAlO, FeTiAlMgO, FeTiAlMnO, and FeTiAlMgMnO at 800 and 900°C, 1–4 kbar, and relatively high oxygen fugacity

Received: 4 August 2005 / Accepted: 22 March 2006 / Published online: 29 June 2006

Abstract A synthetic, low-melting rhyolite composition containing TiO_2 and iron oxide, with further separate additions of MgO, MnO, and MgO + MnO, was used in hydrothermal experiments to crystallize Ilm-Hem and Usp-Mt solid solutions at 800 and 900°C under redox conditions slightly below nickel–nickel oxide (NNO) to ≈ 3 $\log_{10} f_{O_2}$ units above the NNO oxygen buffer. These experiments provide calibration of the FeTi-oxide thermometer + oxygen barometer at conditions of temperature and oxygen fugacity poorly covered by previous equilibrium experiments. Isotherms for our data in Roozeboom diagrams of projected %usp vs. %ilm show a change in slope at $\approx$ 60% ilm, consistent with the second-order transition from FeTi-ordered Ilm to FeTi-disordered Ilm-Hem. This feature of the system accounts for some, but not all, of the differences from earlier thermodynamic calibrations of the thermobarometer. In rhyolite containing 1.0 wt.% MgO, 0.8 wt.% MnO, or MgO + MnO, Usp-Mt crystallized with up to 14% of aluminate components, and Ilm-Hem crystallized with up to 13% geikielite component and 17% pyrophanite component. Relative to the FeTiAlO system, these components displace the ferrite components in Usp-Mt, and the hematite component in Ilm-Hem. As a result, projected contents of ulvöspinel and ilmenite are increased. These changes are attributed to increased non-ideality along joins from end-member hematite and magnetite to their respective Mg- and Mn-bearing titanate and aluminate end-members. The compositional shifts are most pronounced in Ilm-Hem in the range $Ilm_{50–80}$, a solvus region where the chemical potentials of the hematite and ilmenite components are nearly independent of composition. The solvus gap widens with addition of Mg and even further with Mn. The Bacon–Hirschmann correlation of Mg/Mn in Usp-Mt and coexisting Ilm-Hem is displaced toward increasing Mg/Mn in ilmenite with passage from ordered ilmenite to disordered hematite. Orthopyroxene and biotite crystallized in experiments with added MgO and MgO + MnO; their X_{Fe} varies with $\log_{10} f_{O_2}$ and T consistent with equilibria among ferrosilite, annite, and ferrite components, and the chemical potentials of SiO_2 and orthoclase in the liquid. Experimental equilibration rates increased in the order: Opx < Bt < Ilm-Hem < Usp-Mag.

Communicated by J. Hoefs

B. W. Evans (✉) · S. M. Kuehner
Department of Earth and Space Sciences,
University of Washington, Box 351310,
Seattle, WA 98195-1310, USA
E-mail: bwevans@u.washington.edu

B. Scaillet
Institut des Sciences de la Terre d'Orléans,
UMR 6113 CNRS-UO, 1a rue de la Férollerie,
45071 Orleans Cedex 2, France
E-mail: bscaille@cnrs-orleans.fr

Introduction

In this paper we shall conserve space by using abbreviations for minerals and phase-components following Lindsley (1991, Table 1): for example, Usp for ulvöspinel, Usp-Mt for ulvöspinel-magnetite solid solutions, and usp and mt for the ulvöspinel and magnetite components of spinel.

The FeTi-oxide thermometer + oxygen barometer of Buddington and Lindsley (1964) has had unparalleled success as a petrogenetic indicator in natural igneous systems. Derived temperatures and oxygen fugacities have supplied critical constraints for a variety of important issues: magma source regions and their redox states, igneous fractionation paths, equilibria and speciation in volcanic gases, solubilities, igneous mineralogy, and so on. Published applications of the thermobarometer have mostly concerned systems with redox states between those defined by the iron-wüstite and NNO solid oxygen buffers. In these cases, an Usp-Mt solid solution coexists with an Ilm-Hem solid solution

Table 1 Microprobe analyses of glass starting compositions

Composition (wt.%)	I	II	III	IV
SiO_2	74.2	71.1	73.5	73.4
TiO_2	1.36	1.34	1.30	1.24
Al_2O_3	11.06	12.39	11.48	11.38
Fe_2O_3	4.03	4.26	4.01	3.68
FeO	1.56	1.65	1.55	1.41
MnO	0.01	0.13	0.81	0.83
MgO	0.00	1.01	0.03	1.03
Na_2O	3.02	2.65	2.43	2.33
K_2O	4.25	4.55	3.96	4.25
Total	99.49	99.08	99.07	99.55

FeO = 0.3 × total Fe (see text)

that contains more than 85% of the ilm component, thereby occupying a part of composition— $\log_{10} f_{O_2} - T$ space well covered by the laboratory phase-equilibrium brackets used for calibration.

More oxidizing conditions ($f_{O_2} >$ NNO) open composition space to less titaniferous Mt and to more hem-rich Ilm and ilm-rich Hem, and involve passage across the transition curve for the coexistence of the long-range, partially FeTi-ordered $R\bar{3}$ and the long-range disordered $R\bar{3}c$ structures (e.g., Harrison et al. 2000a). Because of the extrapolation required, Andersen and Lindsley (1988) expressed strong reservations about use of their formulation of the thermobarometer outside the range of calibration (NNO and below), although the QUILF software (Andersen et al. 1993) provides the user access to it. The other formulation currently in use (Ghiorso and Sack 1991) in principle accommodates a broader range of compositions, including minor constituents, but it suffers similarly from the paucity of direct experimental brackets for FeTi-oxides equilibrated at $f_{O_2} >$ NNO.

The crystallization products of more oxidized magmas, notably those found in magmatic arcs, include FeTi-oxides with compositions outside the range of experimental calibration. As we pointed out earlier (Evans and Scaillet 1997), application of both the Andersen and Lindsley (1988) and Ghiorso and Sack (1991) formulations of the thermobarometer under these higher f_{O_2} conditions can give estimates of $\log_{10} f_{O_2}$ that are too high and temperatures (depending on the range of $\log_{10} f_{O_2}$) both too high and too low. These problems stem from shortcomings in the calibration of the thermobarometer both in the simple system FeTiO and in more complex systems containing for example Mg, Mn, and Al.

Extension of the thermodynamic calibration to more oxidizing conditions requires sets of end-member and solution properties that satisfactorily reproduce the compositions of coexisting spinel and rhombohedral oxide solid solutions determined in the laboratory under controlled conditions of temperature, pressure, and $\log_{10} f_{O_2}$. Especially important is appropriate provision for the thermodynamic consequences of long-range order in Ilm-Hem, including the accurate location of the order–disorder transition. Furthermore, the presence of additional components greatly increases the matrix of on-site or molecular interaction parameters that need to be known with some reliability, especially in the spinel phase. Each additional component induces unique shifts in the Fe- and Ti-contents of the oxides that cannot be "corrected" by means of simple projections, although much of this has been done in the past. To calibrate the effect of these compositional extensions, we need well-controlled and characterized experiments performed at high oxygen fugacities over a range of temperatures.

We present here the results of hydrothermal experiments at 800 and 900°C designed to calibrate the FeTi-oxide thermobarometer in the redox range ΔNNO = − 0.4 to + 3, where ΔNNO is the calculated $\log_{10} f_{O_2}$ of the experiment, minus that of the NNO oxygen buffer at the same temperature. We take advantage of the fact that the crystallization products of natural volcanic liquids or their synthetic liquid equivalents, held for 1–2 weeks at elevated pressures and temperatures of 800–900°C under H_2O-saturated conditions, consist of assemblages of crystals whose textural relations and generally homogeneous compositions reflect equilibration with each other and the surrounding liquid (Pichavant 1987; Holtz et al. 1992; Scaillet et al. 1995). The FeTi-oxides crystallized in our experiments all contain some Al_2O_3 derived from the synthetic liquid. We also examined the effect of minor components on the FeTi-oxide compositions by separately adding MgO, MnO, and MgO + MnO to our charges.

In a complementary study, Lattard et al. (2005) provided new experimental data for the Fe–Ti oxide thermo-oxybarometer in the system Fe–Ti–O at 1 bar, 1,000, 1,100, 1,200, and 1,300°C, and a wide range of oxygen fugacities. These data will be added to ours and to previous experimental brackets in a thermodynamic formulation in preparation (Ghiorso et al. 2003).

Experimental methods

To promote the diffusion of components within our charges and to maximize the percentage of melt, we chose as starting material a synthetic glass with the composition of a minimum-melting, H_2O-saturated rhyolite. Under the T and P conditions chosen, this composition eliminates any possible crystallization of quartz, K-feldspar, plagioclase, Ca-clinopyroxene, and hornblende. The iron–titanium oxides in our experiments crystallize from the liquid (e.g., Scaillet and Evans 1999) rather than by the slower process of alteration of oxide phases already present in the starting materials.

The minimum-melting rhyolite composition was prepared using a classical gel method. Four compositions of starting material (Table 1) were then prepared by adding (by weight): I—5% FeO (as the nitrate) and 1.3% TiO_2 (as ammonium titanyloxalate), II—a further 1% MgO (as nitrate), III—instead of MgO, a further 0.8% MnO (as carbonate), and IV—a combination of

1% MgO and 0.8% MnO. After drying and firing to eliminate the excess C and N, the gels were melted twice at 1,400°C for 3–4 h in air atmosphere to obtain a dry glass. Table 1 shows that glass II is poorer in SiO_2 and richer in Al_2O_3 than the other three; this was unintended and we think caused by a weighing error. Analyses for FeO in glass I and in other synthetic rhyolite glasses prepared at CNRS Orléans in a similar manner indicate a ratio of 0.3 for Fe^{2+}/total Fe; this proportion has been incorporated in the microprobe data listed in Table 1.

Charges plus excess H_2O were held in sealed Au tubes 15 mm long, 2.5 mm in diameter, and 0.2 mm in wall thickness. Experiments of 5–28 days duration (Table 2) were performed at 800°C in a cold-seal pressure vessel (CSPV) and at 800 and 900°C in an internally heated pressure vessel (IHPV), both equipped with a Shaw-type semi-membrane for the control of H_2 pressure (Scaillet et al. 1992). Capsules containing the four compositions were run simultaneously. Total pressure was monitored by transducers calibrated against a Heise Bourdon tube gauge, with an uncertainty of ±20 bars. Temperature was measured by type-K thermocouples calibrated against the melting point of NaCl, with an overall uncertainty of ±5°C for the IHPV and ±8°C for the CSPV. Run temperatures were reached in about 20 min, after which crystals grew at constant temperature, pressure, and f_{H_2}. Experiments were terminated by switching off the power supply (IHPV), or by removing the vessel from the furnace (CSPV) and cooling it with a small fan, in both cases producing a temperature decrease of 400°C in the first 4 min. A drop quench was used when the CSPV was not fitted with a membrane.

Control of oxygen fugacity during the experiments was achieved by adjusting the hydrogen content of the Ar–H_2 pressure medium (IHPV) or by direct diffusion of H_2 across the membrane under the experimental conditions (CSPV). The pressure of H_2 is known to ±0.1 bars, except for vessels not equipped with a membrane (Table 2), in which case the O_2 pressure (±0.5 log units) is an estimate based on several NiPd-sensor measurements in the same vessel over the previous 5 years. The applied hydrogen pressure is registered by the charge within minutes, and the pressure of H_2O in the charge (and hence oxygen fugacity) equilibrates within some hours as H_2O diffuses in from the grain boundaries of the finely ground, fused starting material. Prior to reaching H_2O-saturation there may be some formation of crystal nuclei, but most of these soon dissolve because of the lower liquidus temperatures at H_2O-saturation. $Log_{10}f_{O_2}$ was calculated from the hydrogen pressure using the MRK-EOS of Holloway (1987) for the H–O system at the experimental pressure and temperature, together with the dissociation constant of H_2O from Robie et al. (1979). The $\log_{10} f_{O_2}$ is then referenced to the NNO buffer (as ΔNNO) after O'Neill and Pownceby (1993). When the H_2 pressure is very low (e.g., ≈1 bar), its uncertainty translates into a ±0.2 uncertainty in ΔNNO. Except where specifically noted (in the 800°C experiments), the results of this study are internally consistent when we allow a ±0.2–0.3 uncertainty in the experimental ΔNNO values.

Microprobe analysis of experimental products

Experimental products consist of crystals of Usp-Mt and Ilm-Hem solid solutions embedded in hydrous synthetic rhyolite glass; compositions II and IV contain

Table 2 Summary of experimental run conditions

Run	T (°C)	P (bars)	P_{H_2} (bars)	$\log f_{O_2}$	ΔNNO	Duration (days)	Vessel
2	909	1,602	(0.51)	−9.24	2.5	13	IHPV
3	800	1,021	(0.28)	−11.38	2.5	15	IHPV
4	800	4,133	3.39	−12.34	1.39	8	IHPV-H_2
5	800	4,083	3.52	−12.39	1.34	7	IHPV-H_2
6	800	2,050	(0.16)	−10.34	3.5	14	CSPV
7	806	2,100	(0.52)	−11.21	2.5	7	IHPV
8	801	2,000	13.90	−14.22	−0.42	26	CSPV-H_2
9	800	1,500	4.00	−13.39	0.45	17	CSPV-H_2
10	800	1,500	3.50	−13.27	0.57	15	CSPV-H_2
11	800	1,064	2.82	−13.35	0.51	11	IHPV-H_2
12	800	1,500	1.20	−12.34	1.50	5(+1)	IHPV-H_2
13	900	2,058	2.20	−10.50	1.38	5	IHPV-H_2
14	900	1,074	1.00	−10.33	1.59	6	IHPV-H_2
15	800	3,910	(0.29)	−10.26	3.45	6	IHPV
16	900	1,281	11.64	−12.32	−0.41	6.5	IHPV-H_2
17	701	2,000	7.10	−16.32	−0.14	28	CSPV-H_2
18	900	1,227	7.20	−11.93	−0.02	6	IHPV-H_2
19	900	1,162	3.92	−11.45	0.47	7	IHPV-H_2
20	900	1,168	1.78	−10.76	1.16	6	IHPV-H_2
21	900	1,290	0.81	−10.00	1.91	8	IHPV-H_2
22	800	1,450	9.15	−14.14	−0.30	16	CSPV-H_2
23	798	1,550	6.80	−13.87	0.01	20	CSPV-H_2
24	800	2,055	12	−14.09	−0.27	15	IHPV-H_2
25	900	1,570	1	−10.02	1.88	6	IHPV-H_2
26	900	1,548	3.7	−11.17	0.73	6	IHPV-H_2

IHPV-H_2 and *CSPV-H_2* internally heated pressure and cold seal pressure vessels fitted with a Shaw membrane

orthopyroxene as well in experiments at 900°C, and biotite (composition II) and orthopyroxene (composition IV) in experiments at 800°C. Phases were analyzed with a 4-wavelength spectrometer JEOL 733 Superprobe at the University of Washington. Instrumental conditions were 15 kV accelerating potential, 10 nA beam current, and a finely focused electron beam. In order to minimize overlap of the beam from FeTi-oxide onto the rhyolite glass, extensive use was made during the analysis of Ilm-Hem grains of digital secondary electron images acquired with a GATAN Digital Micrograph for positioning the electron beam.

Usp-Mt formed cube-octahedral crystals 2–10 μm in cross-section (Fig. 1a), and overlap of the analysis volume with glass was successfully avoided for almost all analytical points. Ilm-Hem formed platy crystals typically 1 μm × 5 μm × 5 μm in size, and a correction for glass overlap was necessary for many of the grains analyzed. Our glass correction incorporates a correction for error introduced by the large density contrast (Warren 1997) between FeTi-oxide (ρ = 4.8–5.3) and glass (ρ = 2.3). Without the density correction, contaminated analysis totals exceed 100%. The hydrous rhyolite glass contains on average 74 wt.% SiO_2 and 11 wt.% Al_2O_3. Analyses of Ilm-Hem including more than 10% glass (7.4 wt.% SiO_2 after density correction, but prior to the overlap correction reducing SiO_2 to 0) were excluded from the database.

Analyses were referenced to a library of standards, including four analyzed natural ilmenites and four synthetic compositions along the join $FeTiO_3$–$MnTiO_3$, Elba hematite, and synthetic and natural rutile. Using the binomial alpha factors (CITZAF) of Armstrong (1988a, 1988b), and a first-approximation estimate of excess oxygen by difference from 100% total, we found for TiO_2 that the use of rutile as standard resulted in analyses of our standard ilmenites that were 1–2% (relative) too high. Similarly, use of the Elba hematite gave analyses of Fe in standard ilmenites that were 1–2% (relative) low. This is further discussed in the Appendix. Use of the PAP instead of the CITZAF correction changed TiO_2 and FeO analyses of ilmenite by 0.2 and 0.1% relative, too small to account for the discrepancies. The final corrected analyses (Tables 3, 4, 5, 6) were optimized to the intensities from the synthetic and natural ilmenites as described in the Appendix.

After assignment of Fe to Fe^{2+} and Fe^{3+} based on ideal stoichiometry, analysis totals average 98.7% (including 0.1% SiO_2) for Usp-Mt and slightly higher for Ilm-Hem (even after correction for glass contamination, some totals are high). Analysis of much larger crystals of FeTi-oxides in natural rock samples under identical instrumental conditions generally produced analysis totals close to 100%. From this comparison, we attribute the systematically low analysis totals of Usp-Mt and most Ilm-Hem to the minor loss of Fe and Ti counts that would have been fluorescence-induced by the continuum in larger crystals at distances from the electron-beam impact point greater than about 5 μm. This

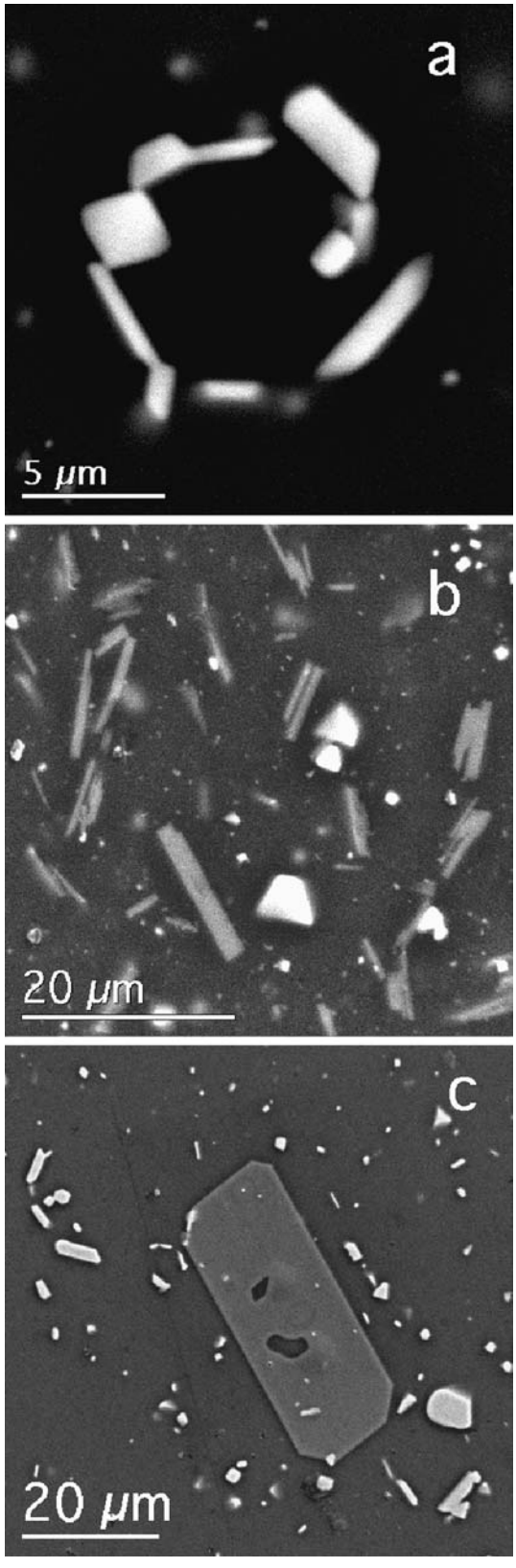

Fig. 1 Secondary electron scanning images. **a** Magnetite (two equant grains) and Ilm-Hem (elongate) in experiment 24 at 800°C, **b** FeTi-oxides (*bright*) and biotite (*gray*) in experiment 24, and **c** orthopyroxene (*gray*), magnetite (equant, *bright*), and Ilm-Hem (elongate, *bright*) in experiment 25

effect was described by Small et al. (1978), and, for example, can be seen in the analyses of experimental FeTi-oxides in Toplis and Carroll (1995). When possible, at least ten grains of both phases were analyzed on each sample, but in a few cases only one or two acceptable analyses of Ilm-Hem were possible, owing to their small grain-size. Measured standard deviations for each element are listed in Tables 3, 4, 5, and 6. Because of covariation in measured Fe, Ti, and analysis totals, standard deviations tend to be smaller when calculated after any kind of normalization, for example, to an analysis total of 100 wt.%, to atom percent Ti/(Ti + Fe), to projected usp and ilm (Tables 3, 4, 5, 6), or to mole fractions of end-members. Neither low nor high analysis totals nor inadequate correction for contamination by glass had any detectable systematic effect on normalized compositions. Obvious compositional outliers among the analyzed spots (e.g., in Al due to inadequate correction for glass, or in Ti/(Ti + Fe) ratio due to overlap with the other FeTi-oxide) were deleted.

Results

Fourteen experiments were conducted at 800°C, ten at 900°C, and an unsuccessful one at 700°C. FeTi-oxides crystallized at 900°C are homogeneous, with 1σ for Fe/(Fe + Ti) smaller than 0.2% for Usp-Mt, and mostly smaller than 0.5% for Ilm-Hem. In the series of experiments at 800°C, Usp-Mt is as homogeneous as at 900°C, whereas the composition of Ilm-Hem is variable, especially when falling in the range Ilm_{50}–Ilm_{80}. The latter show up in Tables 3, 4, 5, and 6 as having standard deviations of Fe/(Fe + Ti) in excess of 1.0%, and in our Roozeboom diagrams (below) as having large uncertainties or wide measured ranges.

The microprobe analyses of both FeTi-phases always show a minimum of 0.1–0.2 wt.% SiO_2, even in the largest crystals present. This silica is inferred to be present in the structures of the two phases.

Normalization

We recast weight percent microprobe analyses to three oxygens and two total cations for Ilm-Hem and four oxygens and three total cations for Usp-Mt. The rhombohedral phase in our experiments may be expressed with no ambiguity in terms of the mole fractions or percentages of five end-members: Al_2O_3, $FeTiO_3$, $MgTiO_3$, $MnTiO_3$, and Fe_2O_3. The spinel phase can be expressed in terms of nine end-members: titanates of Fe, Mg, and Mn; aluminates of Fe, Mg, and Mn; and ferrites of Fe, Mg, and Mn. However, to assign Fe, Mg, and Mn among these requires something that we do not have: knowledge of the fractionation of Fe, Mg, and Mn among the titanate, aluminate, and ferrite end-members in homogeneous equilibrium. Provisionally, we assume that the proportions of Fe, Mg, and Mn are the same in all three end-members.

In our anticipated thermodynamic formulation (Ghiorso et al. 2003; M.S. Ghiorso et al., in preparation), the chemical potentials of end-member components of the temperature-calibration exchange reaction:

$$Fe_2O_3 + Fe_2TiO_4 = FeTiO_3 + Fe_3O_4 \quad (1)$$

and the Fe-oxidation reaction:

$$6Fe_2O_3 = 4Fe_3O_4 + O_2 \quad (2)$$

will be evaluated without having to project compositions into the simple system FeTiO. However, for convenience in presenting the data obtained in this study, we shall project by using the ratio: $FeTiO_3/(FeTiO_3 + Fe_2O_3)$ for the mole fraction of ilmenite [$= Fe^{2+}/(Fe^{2+} + Fe^{3+}/2)$], and the ratio: $Fe_2TiO_4/(Fe_2TiO_4 + Fe_3O_4)$ for the mole fraction of ulvöspinel. Given our assumption about the equal partition of Fe, Mg, and Mn in the spinel, the latter is equivalent to the cation ratio $Ti/(Ti + Fe^{3+}/2)$. We do not mean to imply that this projection is superior to others that have been proposed (e.g., Lindsley and Spencer 1982; Stormer 1983).

Attainment of equilibrium

Because all our experiments involved crystallization of the FeTi-oxides from liquid, that is by synthesis, there is no guarantee that their compositions in run-products represent equilibrium under the experimental conditions of T, P, and f_{O_2}. Bracketing experiments (e.g., Lindsley 1962, 1963; Andersen and Lindsley 1979, 1988; Spencer and Lindsley 1981) are ordinarily considered more reliable indicators of equilibrium, although this inference has been questioned in the case of solid solution reversals fluxed by fluid. According to Pattison (1994), growth of the solids by solution-precipitation rather than lattice diffusion destroys the criterion of bracketing.

In the present case, what is known of the kinetics of equilibration of Usp-Mt, as reviewed in Venezky and Rutherford (1999), and our own experience of composition reversals in the system (Evans and Scaillet 1997), suggest that a reasonable approach to equilibration in experiments of 1–2 weeks duration at 800 and 900°C might be expected, given the dimensions of our oxide crystals, and the fact that they grew from a hydrous silicate liquid. The general homogeneity of run-products in the 900°C series of experiments is consistent with this assertion. Whereas Usp-Mt at 800°C is also generally homogeneous, the Ilm-Hem in some cases is patently not. In a few cases at 800°C, we suspect that non-equilibrium growth of FeTi-oxides at the start of the experiment, prior to equilibration of H_2O, H_2, O_2, and the liquid ferrous/ferric ratio, was not entirely erased by the end of the experiment. For intermediate compositions of Ilm-Hem, the chemical potential driving forces for equilibration of the solid are extremely small.

Analytical uncertainties in terms of projected %usp in analyses of Usp-Mt and projected %ilm in Ilm-Hem are also given in Tables 3, 4, 5, and 6. For Usp-Mt 1σ

Table 3 Microprobe analyses (wt.%) of product FeTi-oxides: Usp-Mt above and Ilm-Hem below—composition I

Experiment no.	8[a]	22[a]	24	23	9	11[a]	10	4	12	3	7	7	18	19	26	20	13	14	25	21	2
Temperature (°C)	801	800	800	798	800	800	800	800	800	800	806	806	900	900	900	900	900	900	900	900	909
Pressure (bars)	2,000	1,450	2,055	1,550	1,500	1,064	1,500	4,133	1,500	1,021	2,100	2,100	1,227	1,162	1,548	1,168	2,058	1,074	1,570	1,290	1,602
ΔNNO	−0.42	−0.30	−0.27	0.01	0.45	0.51	0.57	1.39	1.50	2.5	2.5	2.5	−0.02	0.47	0.73	1.16	1.38	1.59	1.88	1.91	2.50
No. of anal. spots	12	9	12	11	11	10	11	4	10	8	12	5	10	10	11	10	10	10	10	10	9
TiO_2	7.59	4.29	12.64	9.26	6.31	9.38	6.40	4.81	5.09	2.27	3.36	3.00	14.49	13.03	10.82	8.68	7.52	5.61	5.28	5.80	2.40
Al_2O_3	1.68	1.69	1.63	1.81	1.79	1.92	1.82	1.47	1.78	1.94	1.61	1.37	1.83	1.94	1.79	2.01	1.75	2.07	1.92	2.12	2.06
Fe_2O_3	51.44	57.57	41.94	48.48	53.25	47.46	53.51	56.76	55.98	61.97	59.83	59.68	37.74	40.66	44.73	49.36	51.75	55.28	55.50	54.13	59.62
FeO	37.89	34.76	42.70	39.41	36.56	39.58	36.83	35.17	35.56	33.15	33.99	32.96	44.28	43.05	40.79	39.20	37.96	36.38	35.84	36.22	32.53
MnO	0.04	0.01	0.01	0.00	0.00	0.00	0.00	0.00	0.02	0.03	0.08	0.15	0.01	0.02	0.01	0.03	0.01	0.00	0.00	0.02	0.03
MgO	0.03	0.02	0.03	0.05	0.01	0.00	0.02	0.04	0.01	0.01	0.02	0.06	0.02	0.02	0.03	0.01	0.05	0.02	0.03	0.03	0.02
Total	98.67	98.34	98.95	99.01	97.92	98.34	98.58	98.25	98.44	99.37	98.89	97.22	98.37	98.72	98.17	99.29	99.04	99.36	98.57	98.32	96.66
1σ wt.% to second decimal place																					
TiO_2	6	12	13	9	14	25	16	7	9	12	19	20	19	14	8	5	9	10	6	9	7
Al_2O_3	4	7	3	5	6	8	3	4	3	3	18	10	2	4	4	2	5	8	3	4	27
Fe_2O_3	21	34	39	31	44	70	68	15	78	73	100	81	46	39	36	34	37	23	52	19	107
FeO	7	25	18	13	15	57	21	18	30	34	57	45	23	23	11	18	12	16	23	16	32
MnO	2	2	1	0	0	1	0	0	2	2	12	3	1	1	1	2	1	0	0	2	2
MgO	2	1	1	2	1	0	1	5	1	1	3	1	1	1	1	1	2	1	1	1	1
1σ Ti/(Ti + Fe) at.%	0.06	0.10	0.14	0.10	0.15	0.20	0.18	0.07	0.12	0.13	0.19	0.19	0.19	0.14	0.10	0.06	0.11	0.10	0.07	0.08	0.08
usp% proj.	22.77	12.96	37.59	27.63	19.15	28.32	19.29	14.48	15.38	6.82	10.09	9.13	43.42	39.04	32.59	26.01	22.51	16.86	15.98	17.64	7.45
1σ usp% proj.	0.19	0.31	0.43	0.28	0.45	0.61	0.56	0.19	0.36	0.39	0.60	0.57	0.58	0.42	0.31	0.18	0.32	0.28	0.22	0.24	0.26
No. of anal. spots	10	7	10	9	9	3	10	8	7	7	3	8	5	9	10	10	10	7	10	9	12
TiO_2	38.84	24.70	45.91	43.51	34.69	42.15	33.94	27.62	28.03	19.42	24.32	22.97	43.67	42.54	39.94	30.84	29.06	26.02	25.75	26.21	18.60
Al_2O_3	0.23	0.42	0.19	0.25	0.38	0.38	0.35	0.37	0.72	0.58	0.25	0.59	0.37	0.24	0.31	0.60	0.51	0.69	0.55	0.56	0.61
Fe_2O_3	24.24	51.15	12.07	16.68	32.21	18.00	34.50	46.32	46.81	62.16	51.73	56.29	15.94	18.22	22.97	41.08	43.21	49.66	49.57	48.07	61.77
FeO	34.84	22.20	41.21	39.01	31.15	37.83	30.46	24.80	25.20	17.29	21.75	20.51	39.22	38.16	35.87	27.68	26.05	23.35	23.10	23.56	16.69
MnO	0.04	0.00	0.02	0.00	0.03	0.03	0.02	0.02	0.00	0.01	0.05	0.09	0.01	0.04	0.01	0.00	0.00	0.00	0.01	0.00	0.01
MgO	0.03	0.01	0.03	0.06	0.01	0.03	0.02	0.01	0.00	0.01	0.03	0.03	0.02	0.03	0.02	0.03	0.05	0.03	0.03	0.01	0.02
Total	98.22	98.48	99.43	99.51	98.47	98.42	99.29	99.14	100.76	99.47	98.13	100.48	99.23	99.23	99.12	100.23	98.88	99.75	99.01	98.41	97.70
1σ wt.% to second decimal place																					
TiO_2	71	16	39	19	39	79	45	41	160	17	42	76	76	64	37	44	32	18	28	24	17
Al_2O_3	8	3	8	8	11	2	6	7	27	15	13	15	18	3	10	12	17	12	9	7	2
Fe_2O_3	74	72	65	97	160	34	35	128	283	72	138	101	95	68	29	130	38	72	79	97	72
FeO	66	15	37	19	34	69	42	35	144	12	48	67	68	59	33	39	29	16	25	22	15
MnO	3	0	2	0	2	2	2	2	0	1	5	3	2	1	1	1	0	0	1	0	1
MgO	2	1	1	1	1	1	1	1	1	1	4	4	1	1	1	1	2	1	1	1	1
1σ Ti/(Ti + Fe) at.%	0.25	0.24	0.29	0.40	0.61	0.11	0.18	0.28	1.39	0.19	0.44	0.57	0.29	0.27	0.13	0.25	0.17	0.11	0.14	0.29	0.20
ilm% proj.	76.16	49.10	88.36	83.87	68.25	82.37	66.24	54.34	54.47	38.20	48.31	44.75	84.54	82.32	77.63	59.96	57.26	51.10	50.88	52.14	37.52
1σ ilm% proj.	0.51	0.49	0.36	0.82	1.20	0.17	0.38	0.76	2.78	0.22	1.23	1.12	0.59	0.54	0.24	0.51	0.32	0.22	0.28	0.58	0.41

Proj. projected as described in the text

[a]ΔNNO value unreliable. Analysis totals do not include approx. 0.1% SiO_2

Table 4 Microprobe analyses (wt.%) of product FeTi-oxides: Usp-Mt above and Ilm-Hem below—composition II

Experiment no.	22[a]	24	9	11[a]	10	5	4	12	3	7	16	18	19	26	20	13	14	25	21	2
Temperature (°C)	800	800	800	800	800	800	800	800	800	806	900	900	900	900	900	900	900	900	900	909
Pressure (bars)	1,450	2,055	1,500	1,064	1,500	4,083	4,133	1,500	1,021	2,100	1,281	1,227	1,162	1,548	1,168	2,058	1,074	1,570	1,290	1,602
ΔNNO	−0.30	−0.27	0.45	0.51	0.57	1.34	1.39	1.50	2.5	2.5	−0.41	−0.02	0.47	0.73	1.16	1.38	1.59	1.88	1.91	2.5
No. of anal. spots	10	11	10	3	10	10	7	10	3	10	10	11	9	10	10	10	10	10	10	10
TiO_2	4.91	12.53	8.43	8.95	8.06	5.50	5.16	5.59	2.83	3.90	16.53	14.45	12.97	11.23	9.66	8.38	6.98	6.67	7.27	3.59
Al_2O_3	4.89	4.27	5.05	5.73	5.25	3.41	3.31	5.33	6.05	4.49	4.16	4.53	4.97	4.48	4.94	3.83	5.38	4.75	5.47	4.77
Fe_2O_3	54.05	40.14	46.03	44.72	47.54	53.61	54.99	51.10	56.92	55.94	32.42	35.74	38.43	42.26	45.23	48.58	49.93	50.87	49.34	56.83
FeO	33.13	41.70	37.07	37.76	36.89	34.75	34.48	34.46	31.63	32.89	43.86	41.52	40.20	38.32	35.95	35.41	33.13	32.91	33.28	28.84
MnO	0.25	0.18	0.18	0.22	0.16	0.09	0.12	0.16	0.20	0.20	0.14	0.12	0.16	0.17	0.18	0.16	0.17	0.14	0.14	0.22
MgO	1.81	0.97	1.22	1.28	1.43	0.88	0.98	1.22	1.78	1.26	1.82	2.03	2.10	2.17	2.85	2.27	3.09	2.91	3.20	3.55
Total	99.04	99.79	97.98	98.66	99.33	98.24	99.04	97.86	99.41	98.68	98.93	98.39	98.83	98.63	98.81	98.63	98.68	98.25	98.70	97.80
1σ wt.% to second decimal place																				
TiO_2	6	11	14	7	17	10	11	9	13	19	18	13	11	12	7	13	10	7	6	4
Al_2O_3	9	4	10	28	10	12	4	6	43	10	8	12	10	8	7	9	9	3	7	7
Fe_2O_3	60	37	52	49	14	49	60	21	160	82	55	45	50	47	55	32	31	31	36	31
FeO	24	25	17	29	34	24	21	10	86	37	23	23	17	27	20	25	24	13	16	11
MnO	4	2	3	3	3	7	5	3	5	8	2	2	3	2	3	3	3	2	1	2
MgO	4	7	5	4	6	4	2	4	23	8	3	10	4	5	8	7	5	5	7	4
1σ Ti/(Ti + Fe) at.%	0.08	0.10	0.16	0.04	0.14	0.10	0.13	0.10	0.16	0.21	0.22	0.10	0.16	0.12	0.08	0.14	0.08	0.07	0.08	0.05
usp% proj.	15.37	38.42	26.80	28.57	25.31	17.02	15.79	17.94	9.04	12.23	50.47	44.69	40.28	34.69	29.92	25.64	21.84	20.76	22.75	11.21
1σ usp% proj.	0.25	0.32	0.51	0.20	0.41	0.27	0.41	0.30	0.49	0.63	0.66	0.34	0.47	0.37	0.23	0.41	0.25	0.21	0.24	0.15
No. of anal. spots	8	4	4	1	3	10	8	1	9	9	11	10	7	10	10	10	8	10	10	10
TiO_2	31.95	48.64	45.82	44.30	43.78	30.54	29.42	37.13	23.27	27.17	47.00	45.65	45.69	44.63	40.90	38.83	30.33	29.58	30.55	22.64
Al_2O_3	0.81	0.49	0.73	0.81	0.62	0.63	0.60	1.72	1.16	0.97	0.49	0.57	0.61	0.48	0.71	0.61	0.99	0.88	1.07	1.02
Fe_2O_3	41.10	10.79	14.35	19.00	19.47	40.44	43.16	27.88	56.88	52.41	11.17	14.85	15.35	16.42	23.86	26.23	42.46	43.47	41.87	55.13
FeO	25.16	40.53	37.19	36.04	34.70	25.56	24.66	30.04	18.70	22.26	37.75	35.67	35.64	34.54	30.44	30.05	23.04	22.48	22.87	16.49
MnO	0.10	0.23	0.21	0.28	0.22	0.08	0.06	0.19	0.09	0.09	0.17	0.14	0.17	0.19	0.18	0.15	0.06	0.08	0.09	0.07
MgO	1.95	1.67	2.13	1.97	2.50	1.02	0.97	1.77	1.20	1.16	2.44	2.94	2.96	3.03	3.45	2.65	2.34	2.27	2.53	2.13
Total	101.07	102.35	100.43	102.40	101.29	98.27	98.87	98.73	101.30	104.06	99.02	99.82	100.42	99.29	99.54	98.52	99.22	98.76	98.98	97.48
1σ wt.% to second decimal place																				
TiO_2	90	58	107		49	109	128		112	86	50	71	59	30	78	51	33	31	32	9
Al_2O_3	14	9	45		12	11	11		16	24	16	27	15	10	17	12	14	8	9	3
Fe_2O_3	184	74	220		182	175	125		240	113	73	78	159	33	61	100	150	63	103	37
FeO	66	50	50		38	83	104		88	66	36	61	79	31	72	33	44	25	39	11
MnO	3	3	2		5	2	2		3	3	3	2	3	6	2	2	3	2	3	2
MgO	21	5	38		27	11	6		10	8	10	12	17	2	18	21	22	7	9	4
1σ Ti/(Ti + Fe) at.%	0.91	0.29	0.56		0.50	1.02	0.88		0.39	0.29	0.33	0.25	0.64	0.18	0.21	0.26	0.31	0.17	0.27	0.06
ilm% proj.	57.64	89.30	85.21	80.83	79.84	58.42	55.95	70.54	42.22	48.56	88.25	84.22	83.77	82.38	73.93	71.80	54.67	53.48	54.83	39.93
1σ ilm% proj.	1.59	0.61	1.84		1.54	1.81	1.65		0.64	0.58	0.63	0.60	1.55	0.35	0.80	0.81	1.08	0.33	0.80	0.24

Proj. projected as described in the text

[a]ΔNNO value unreliable. Analysis totals do not include approx. 0.1% SiO_2

Table 5 Microprobe analyses (wt.%) of product FeTi-oxides: Usp-Mt above and Ilm-Hem below—composition III

Experiment no.	8[a]	22[a]	24	23	9	11[a]	10	5	4	12	3	7	16	18	19	26	20	13	14	25	21	2
Temperature (°C)	801	800	800	798	800	800	800	800	800	800	800	806	900	900	900	900	900	900	900	900	900	909
Pressure (bars)	2,000	1,450	2,055	1,550	1,500	1,064	1,500	4,083	4,133	1,500	1,021	2,100	1,281	1,227	1,162	1,548	1,168	2,058	1,074	1,570	1,290	1,602
ΔNNO	−0.42	−0.30	−0.27	0.01	0.45	0.51	0.57	1.34	1.39	1.50	2.5	2.5	−0.41	−0.02	0.47	0.73	1.16	1.38	1.59	1.88	1.91	2.5
No. of anal. spots	9	9	8	9	9	11	10	8	4	10	5	7	10	10	10	10	10	10	10	10	10	10
TiO_2	8.53	5.56	13.13	9.78	7.28	9.90	7.24	6.53	6.30	6.35	3.90	4.93	17.17	14.90	13.38	11.71	10.21	8.98	7.59	7.34	7.76	4.10
Al_2O_3	4.34	4.80	4.07	4.94	4.94	5.29	4.84	3.47	3.26	5.14	6.28	4.47	3.63	3.99	4.30	3.94	4.35	3.65	4.77	4.24	4.86	4.52
Al_2O_3	46.79	51.49	38.90	43.68	48.36	43.31	48.65	50.17	52.20	49.45	53.13	53.65	30.75	34.74	37.19	40.54	43.48	46.30	48.11	48.55	47.54	54.45
FeO	35.16	31.71	39.66	36.40	33.71	36.22	33.84	33.34	33.23	32.87	29.62	31.79	42.80	40.63	39.17	37.77	36.15	35.53	33.57	33.09	33.53	29.50
MnO	4.21	4.59	4.11	4.06	4.39	4.52	4.24	3.29	3.58	4.21	5.45	4.14	4.26	4.39	4.39	4.14	4.59	3.81	4.79	4.68	4.95	5.28
MgO	0.02	0.10	0.10	0.11	0.10	0.12	0.12	0.05	0.14	0.09	0.12	0.10	0.09	0.09	0.12	0.08	0.12	0.10	0.13	0.12	0.14	0.12
Total	99.05	98.25	99.97	98.97	98.78	99.36	98.93	96.85	98.71	98.11	98.50	99.08	98.70	98.74	98.55	98.18	98.90	98.37	98.96	98.02	98.78	97.97
1σ wt.% to second decimal place																						
TiO_2	3	5	9	16	14	15	8	8	8	7	13	19	19	17	11	5	7	11	4	8	8	4
Al_2O_3	6	8	9	6	28	42	8	14	16	12	19	11	6	9	4	5	5	5	7	4	7	6
Fe_2O_3	35	31	22	49	59	182	41	70	24	35	49	95	45	30	28	25	47	25	33	26	28	29
FeO	20	16	16	30	36	70	30	50	12	23	31	27	27	32	25	18	19	18	18	19	16	16
MnO	4	12	5	0	7	13	7	25	14	11	13	11	7	8	12	7	9	5	9	8	11	6
MgO	2	1	1	4	1	1	2	1	6	1	3	4	1	1	2	1	1	1	1	2	1	1
1σ Ti/(Ti + Fe) at.%	0.04	0.06	0.08	0.15	0.09	0.18	0.08	0.10	0.10	0.09	0.11	0.24	0.19	0.13	0.10	0.07	0.12	0.10	0.05	0.08	0.11	0.05
usp% proj.	26.70	17.75	40.28	30.92	23.13	31.36	22.93	20.64	19.43	20.42	12.79	15.52	52.74	46.16	41.83	36.60	31.94	27.94	23.97	23.21	24.60	13.08
1σ usp% proj.	0.12	0.18	0.26	0.45	0.24	0.64	0.23	0.34	0.25	0.26	0.30	0.70	0.56	0.35	0.28	0.19	0.34	0.31	0.13	0.24	0.29	0.15
No. of anal. spots	10	8	9	11	4	4	7	9	7	1	10	8	3	10	10	10	9	10	9	10	10	10
TiO_2	44.41	40.46	47.64	46.35	44.30	46.16	42.61	37.33	40.28	40.31	25.09	29.84	47.41	45.45	45.44	44.63	40.76	40.05	33.79	29.26	30.50	22.71
Al_2O_3	0.27	0.35	0.32	0.33	0.40	0.49	0.45	0.57	0.45	0.73	1.12	0.62	0.38	0.35	0.31	0.34	0.50	0.52	0.80	0.83	0.74	0.93
Fe_2O_3	14.05	22.28	9.12	11.20	14.40	10.63	17.50	28.30	23.12	22.16	52.61	44.91	9.14	11.10	12.25	13.90	20.93	22.27	35.85	42.21	40.32	53.54
FeO	32.45	28.86	35.88	33.98	32.04	33.68	30.73	28.94	30.38	29.87	19.70	23.49	36.68	34.75	34.30	33.89	30.80	30.91	26.15	23.66	24.39	18.17
MnO	7.20	7.12	6.63	7.32	7.42	7.45	7.28	4.40	5.52	6.07	2.62	3.20	5.69	5.84	6.22	5.87	5.53	4.83	3.96	2.46	2.84	2.09
MgO	0.11	0.18	0.14	0.16	0.16	0.16	0.13	0.04	0.14	0.13	0.12	0.06	0.10	0.12	0.15	0.15	0.14	0.12	0.13	0.09	0.09	0.07
Total	98.49	99.25	99.73	99.34	98.72	98.57	98.70	99.58	99.89	99.27	101.26	102.12	99.40	97.61	98.67	98.78	98.66	98.70	100.68	98.51	98.88	97.51
1σ wt.% to second decimal place																						
TiO_2	38	43	63	83	38	32	48	319	81		34	288	8	79	20	45	78	63	76	34	32	15
Al_2O_3	6	3	15	9	10	10	13	10	30		25	27	15	10	4	8	14	9	10	8	26	3
Fe_2O_3	84	109	50	113	90	76	60	567	112		133	470	85	78	48	32	73	62	107	70	71	33
FeO	31	34	45	70	34	35	45	171	55		27	179	6	57	23	43	64	58	61	29	25	16
MnO	21	29	22	24	12	26	13	164	34		15	82	8	19	10	10	14	13	13	4	9	5
MgO	11	1	1	2	2	1	2	35	3		3	5	2	2	5	1	1	2	1	1	2	1
1σ Ti/(Ti + Fe) at.%	0.42	0.64	0.16	0.55	0.370	0.62	0.33	3.20	0.59		0.30	2.68	0.40	0.30	0.23	0.18	0.26	0.20	0.57	0.18	0.23	0.11
ilm% proj.	83.70	74.22	89.74	87.09	83.18	87.57	79.60	69.45	74.49	74.98	45.42	53.76	89.92	87.43	86.16	84.42	76.59	75.52	61.85	55.47	57.35	43.00
1σ ilm% proj.	0.90	0.99	0.74	1.29	0.90	0.73	0.54	5.17	0.88		0.58	4.27	0.85	0.74	0.53	0.37	0.57	0.62	1.13	0.38	0.47	0.30

Proj. projected as described in the text

[a]ΔNNO value unreliable. Analysis totals do not include approx. 0.1% SiO_2

Table 6 Microprobe analyses (wt.%) of product FeTi-oxides: Usp-Mt above and Ilm-Hem below—composition IV

Experiment no.	22[a]	24	23	9	11[a]	10	5	4	7	16	18	19	26	20	13	14	25	21	2
Temperature (°C)	800	800	798	800	800	800	800	800	806	900	900	900	900	900	900	900	900	900	909
Pressure (bars)	1,450	2,055	1,550	1,500	1,064	1,500	4,083	4,133	2,100	1,281	1,227	1,162	1,548	1,168	2,058	1,074	1,570	1,290	1,602
ΔNNO	−0.30	−0.27	0.01	0.45	0.51	0.57	1.34	1.39	2.5	−0.41	−0.02	0.47	0.73	1.16	1.38	1.59	1.88	1.91	2.5
No. of anal. spots	9	10	6	6	3	8	9	6	5	10	11	10	10	10	10	9	9	10	10
TiO_2	5.67	13.16	9.85	9.11	9.89	8.91	6.68	6.37	5.14	17.50	15.44	14.25	12.02	10.83	9.50	8.26	8.11	8.69	5.02
Al_2O_3	4.39	4.20	4.79	4.68	5.32	4.81	3.15	3.05	3.92	3.35	3.93	4.14	3.71	4.08	3.38	4.46	3.87	4.43	4.09
Fe_2O_3	53.11	38.90	44.35	45.03	42.70	46.04	51.29	52.64	54.02	31.22	34.64	36.50	41.12	44.16	46.66	48.13	48.84	47.59	54.48
FeO	30.18	39.81	36.02	34.59	35.57	34.36	32.86	32.59	30.47	42.03	39.80	38.14	36.16	34.23	33.95	31.14	30.89	31.21	26.68
MnO	3.90	2.90	3.11	3.49	3.26	3.56	2.74	2.90	3.82	3.37	3.64	3.68	3.66	4.05	3.41	4.15	4.18	4.39	4.80
MgO	1.72	0.78	1.05	1.02	1.05	1.22	0.94	0.99	1.11	1.37	1.48	1.74	1.61	2.18	1.72	2.42	2.34	2.53	2.74
Total	98.97	99.75	99.17	97.92	97.79	98.90	97.66	98.54	98.48	98.84	98.93	98.45	98.28	99.53	98.62	98.56	98.23	98.84	97.81
1σ wt.% to second decimal place																			
TiO_2	11	13	8	35	4	13	15	14	30	18	16	15	10	9	9	9	8	10	4
Al_2O_3	4	7	13	18	21	8	10	6	13	5	8	8	4	3	5	9	4	4	4
Fe_2O_3	52	50	24	45	18	24	58	53	64	30	38	52	36	39	28	36	22	33	37
FeO	23	17	18	69	15	31	37	27	59	22	25	23	20	12	13	16	20	25	17
MnO	15	5	17	11	9	7	19	4	30	6	9	13	5	7	5	7	9	9	8
MgO	5	3	18	5	8	5	6	4	13	4	4	3	3	4	3	4	4	5	3
1σ Ti/(Ti + Fe) at.%	0.13	0.15	0.09	0.22	0.06	0.10	0.16	0.15	0.29	0.16	0.13	0.18	0.12	0.11	0.10	0.10	0.08	0.08	0.05
usp% proj.	17.59		30.74	28.79	31.64	27.89	20.65	19.48	15.98	52.84	47.11	43.83	36.88	32.89	28.92	25.54	24.92	26.74	15.55
1σ usp% proj.	0.35	0.47	0.19	0.60	0.13	0.29	0.49	0.44	0.81	0.47	0.39	0.56	0.32	0.35	0.27	0.28	0.24	0.25	0.15
No. of anal. spots	6	4	4	1	1	2	10	7	12	10	7	2	5	3	4	3	10	6	11
TiO_2	42.78	48.67	47.38	46.78	50.29	48.42	41.56	41.97	43.50	48.12	47.41	46.92	46.60	43.22	43.15	41.81	39.55	40.66	24.71
Al_2O_3	0.42	0.38	0.68	0.72	1.69	0.65	0.44	0.49	1.01	0.31	0.39	0.41	0.58	0.65	0.52	0.46	0.57	0.55	0.83
Fe_2O_3	21.77	9.75	13.78	13.27	18.73	18.29	22.68	20.57	35.59	8.56	10.99	13.52	14.50	20.48	19.98	24.92	26.17	24.97	52.05
FeO	27.47	37.07	33.93	33.13	35.64	33.80	30.16	29.84	26.93	35.21	34.14	33.02	32.52	28.44	29.89	27.13	25.76	25.99	16.78
MnO	6.02	4.48	5.66	5.71	6.39	6.03	4.27	4.67	7.58	4.54	4.84	4.68	5.16	5.05	4.39	5.01	4.58	5.02	2.08
MgO	2.75	1.22	1.65	1.76	1.74	2.04	1.62	1.78	2.53	1.95	2.01	2.49	2.34	2.98	2.51	3.03	2.90	3.08	1.87
Total	101.21	101.57	103.08	101.37	114.48	109.23	100.73	99.32	117.14	98.69	99.78	101.04	101.70	100.82	100.44	102.36	99.53	100.27	98.32
1σ wt.% to second decimal place																			
TiO_2	29	61	91			36	206	55	724	61	50	34	75	184	38	50	70	29	12
Al_2O_3	5	11	27			23	18	11	42	8	10	3	29	28	7	8	14	14	4
Fe_2O_3	135	56	58			11	397	138	962	79	104	43	57	218	102	23	65	90	87
FeO	35	53	80			44	145	76	496	45	28	5	65	207	45	42	69	34	9
MnO	21	6	21			27	37	11	192	18	23	13	13	12	17	14	14	5	4
MgO	12	3	10			22	12	20	27	11	10	7	5	19	3	1	16	11	3
1σ Ti/(Ti + Fe) at.%	0.62	0.25	0.32			0.08	2.22	0.51	5.57	0.51	0.48	0.05	0.29	1.04	0.39	0.21	0.30	0.33	0.19
ilm% proj.	73.72	89.42	84.55	84.73	80.88	80.42	74.72	76.33	62.71	90.14	87.35	84.44	83.29	75.53	76.88	70.76	68.63	69.82	41.74
1σ ilm% proj.	1.31	0.46	0.77			0.11	4.09	1.60	10.41	0.79	1.01	0.40	0.40	3.34	1.03	0.45	0.89	1.01	0.40

Proj. projected as described in the text

[a]ΔNNO value unreliable. Analysis totals do not include approx. 0.1% SiO_2

values average 0.30% usp at 900°C and 0.39% usp at 800°C. For Ilm-Hem, 1σ values at 900°C are in the range 0.2–1.5% ilm, and at 800°C they are in the range 0.2–5.2% ilm. The largest uncertainties are for rhombohedral oxides in the near-solvus composition range $ilm_{50–75}$. These high values are not analytical uncertainties but reflect instead real grain-to-grain inhomogeneities.

Systematic compositional differences among the run-products of the four different bulk compositions of starting material in each experiment indicate a reproducibility consistent with equilibrium. This is shown especially well at 900°C by the regular sequence of projected %usp of spinel and almost as well by projected %ilm of the rhombohedral oxide when plotted against experimental ΔNNO (Fig. 2). In both cases the sequence is one of increasing projected %usp and %ilm through compositions I–IV. Similar shifts are found when the projection method of Stormer (1983) is used. By their relative smoothness, the trends in Fig. 2 also provide general indications of the reproducibility of the measured ΔNNO.

Experiments containing both Mg and Mn (bulk composition IV) provide an independent test of the degree of exchange equilibrium between the two oxides crystallized. Our 800 and 900°C data define a line that is ≈0.05 log units of Mg/Mn in Usp-Mt greater than the best-fit line of Bacon and Hirschmann (1988) for natural FeTi-oxide pairs (Fig. 3). We interpret the linear trend to indicate that exchange equilibrium of Mg and Mn

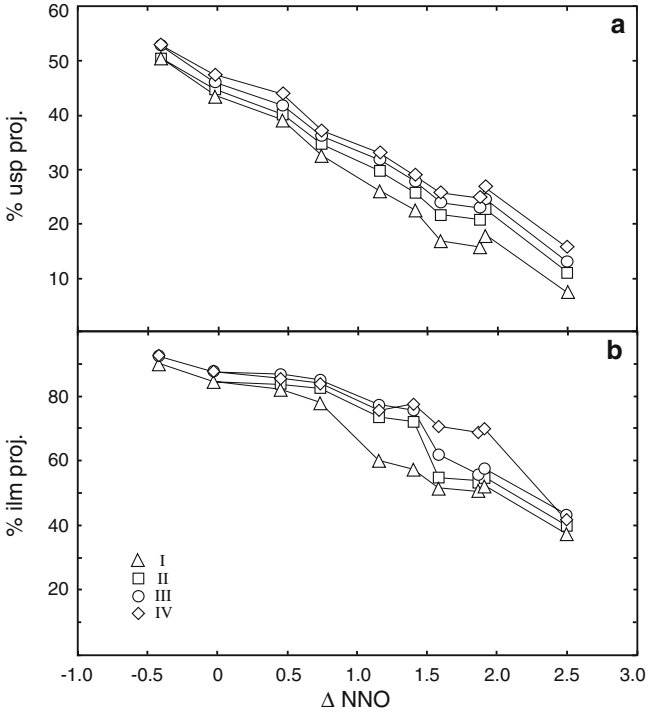

Fig. 2 Projected %usp in spinel (**a**) and projected %ilm in rhombohedral oxide (**b**) vs. ΔNNO in experiments at 900°C for the bulk compositions I, II, III, and IV. *Connecting lines* are for display purposes only

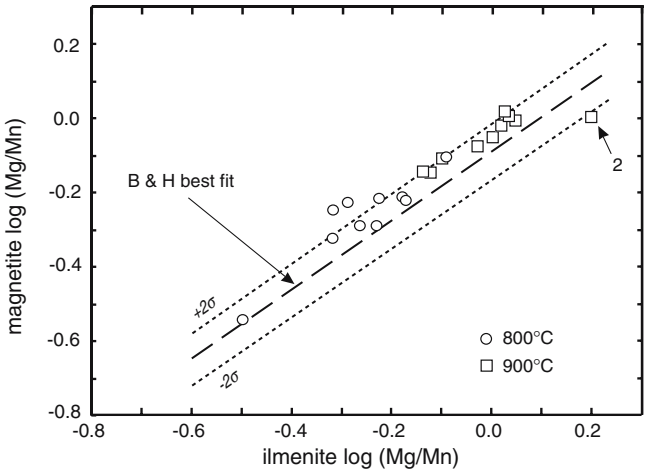

Fig. 3 Log(Mg/Mn) in Usp-Mt vs. log(Mg/Mn) in Ilm-Hem in bulk composition IV. Best fit and 2σ for natural pairs from Bacon and Hirschmann (1988, Fig. 1). Experiment 2 has 53 wt.% hem in Ilm-Hem (see text)

was attained in the majority of our experiments. The small upward displacement relative to the fit of Bacon and Hirschmann may be attributed to the influence of 3.2–5.7 wt.% Al_2O_3 (Tables 3, 4, 5, 6) on uptake of MgO into the Usp-Mt (Lindsley 1991), compared to 0.24–1.03 wt.% Al_2O_3 in Ilm-Hem, and the generally smaller amounts of Al_2O_3 in most of the natural oxide pairs. Despite its location (Fig. 3) experiment 2 was also in Mg/Mn exchange equilibrium. The increase in Mg/Mn in Ilm-Hem results from the passage from FeTi-ordered ilmenite to disordered hematite, as explained later under "Bulk composition III."

It has been suggested that the relatively high Al_2O_3 contents of both FeTi-oxides in our experiments may in part be attributed to kinetic problems (such as sluggish diffusion of Al in the liquid). We believe this to be unlikely for the following reasons. In similar experiments on a glass of Pinatubo dacite (Scaillet and Evans 1999), the average Al_2O_3 content of Usp-Mt in six experiments at ΔNNO from 1.04 to 1.71 and T = 776 and 834°C was 2.20 wt.% (analyses revised from 1999), as compared to an average of 1.94 wt.% Al_2O_3 in 14 published analyses of natural Pinatubo magnetite. An average of 0.51 wt.% Al_2O_3 in Ilm-Hem in the same six experiments compares with an average of 0.37 wt.% in the natural Pinatubo ilmenites. These differences are not large and may well reflect the influence of temperature on the uptake of Al_2O_3 in the FeTi-oxides in natural silicate liquids. The comparisons provide little compelling evidence of a kinetic problem with respect to the levels of Al.

Three experiments at 800°C (8, 11, and 22) produced oxide Ti/(Ti + Fe) ratios inconsistent with those in experiments under nearby redox conditions. Although apparent failures in terms of redox calibration, these experiments nonetheless provide potential thermometric calibration, and they supply information with respect to relative equilibration rates at 800°C in crystallization experiments of the present kind, as discussed below.

Experiment 8 showed signs of contamination by Ni from a NiPd capsule added to monitor the f_{O_2} and by a capsule containing a foreign sample. This is the likely cause of inconsistent values of ΔNNO among the four compositions and its variation with time during the experiment. The nominal f_{O_2} (ΔNNO = −0.42, Table 2) must be considered unreliable. Ilm-Hem in composition I varies from Ilm_{60} to Ilm_{80}; we tentatively interpret a concentration of compositions at Ilm_{76} to be that in equilibrium with the much more homogenous Usp-Mt, although the ilm-rich extreme seems to fit our isotherm better (Fig. 4). Composition II appears to have been contaminated, although not by Ni; an apparently low f_{O_2} produced an Hc-rich Usp-Mt spinel (with 3 wt.% ZnO!) + Usp-Mt, instead of Ilm-Hem + Usp-Mt. Composition III was Ni-contaminated along one side of the charge, where Usp-Mt was found to contain up to 13 wt.% NiO. Element correlations in these Ni-bearing magnetites show that the addition of Ni has the same effect on the composition of Usp-Mt in a rhyolite host as the addition of Mg and Mn (see below): an increase in TiO_2 and Al_2O_3, and decreases in FeO and Fe_2O_3. Extreme Ni contamination eliminated Ilm, increased Fe_2O_3 and further increased Al_2O_3 in the magnetite. The rest of the charge was not affected, and the oxide compositions seem reasonable (Tables 3, 4, 5, 6). Ilm-Hem in composition IV appeared not to have achieved equilibrium (Ti too low) with the Usp-Mt; this data-point was deleted from our summary of results.

In the products of experiment 11 (ΔNNO = 0.51), %usp and %ilm are within experimental error the same as in experiment 23 (ΔNNO = 0.01). Usp-Mt in experiment 11 is both tabular as well as equant, which suggests pseudomorphic replacement of early-grown Ilm-Hem by Usp-Mt as a result of a 0.5 decrease in oxygen fugacity during the run and the progress of reaction 2.

Experiment 22 at 800°C, nominally at ΔNNO = −0.30 (Table 2), produced FeTi-oxides indicative of higher values of ΔNNO when compared to experiments at nearby ΔNNO. The %usp and %ilm values are out-of-place in this respect for all four bulk compositions, and lie close to those for experiments 4, 5, and 12 (ΔNNO = 1.39, 1.34, and 1.50, respectively). On the other hand, the 40% ferrosilite in orthopyroxene grown in composition IV (see below) is not inconsistent with the nominal ΔNNO. We infer that leakage of fluid took place in the course of this experiment; the orthopyroxene, once crystallized, did not change composition to reflect the increasing f_{O_2} whereas the FeTi-oxides and the biotite [Fe/(Fe + Mg) = 0.34 in composition II, see below] apparently did.

In general the Fe/Mg ratio of the product silicates, orthopyroxene, and biotite, reflect the log f_{O_2} of the fluid. However, the orthopyroxenes are not homogeneous in their Fe/Mg ratios in every experiment (for example 16, 20, and 21 at 900°C and 12 at 800°C), and, where not, the cores of crystals are poorer in Fe than the rims. This suggests that in some cases crystallization of orthopyroxene began to take place in the few hours before the desired run conditions of log f_{O_2} were reached (H_2O, H_2, and O_2 not yet equilibrated). Once crystallized, lattice diffusion in orthopyroxene was sufficiently slow to prevent establishment of final equilibration with the liquid.

Our observations on "problem" experiments suggest that overall equilibration rates were in the order: Usp-Mt > Ilm-Hem > biotite > orthopyroxene.

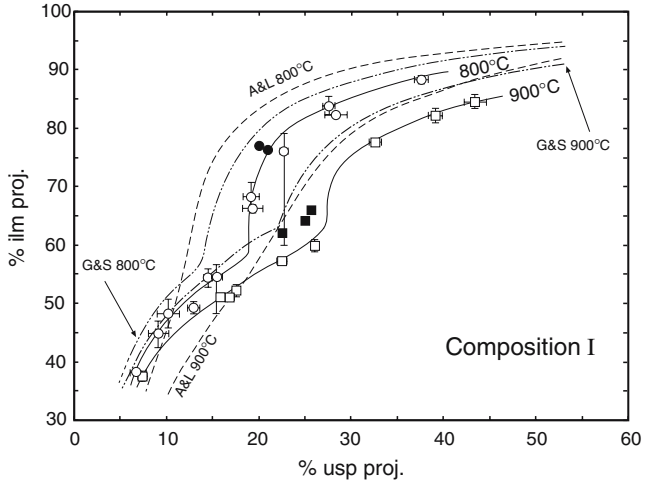

Fig. 4 Roozeboom plot of projected %ilm vs. %usp in experiments on composition I at 800°C (*circles*) and 900°C (*squares*). *Error bars* are $\pm 2\sigma$ or actual range when large and skewed. *Continuous lines* are hand-drawn fits to our data. Also shown are 800 and 900°C isotherms for the pure system FeTiO from the formulations of Andersen and Lindsley (1988) and Ghiorso and Sack (1991). Two experiments (800 and 890°C) on the HAMQ buffer are shown by *filled circles* and *filled squares*, respectively

Bulk composition I (FeTiAlO system)

Isotherms drawn in Roozeboom diagrams (e.g., Ghiorso and Sack 1991, Fig. 5; Evans and Scaillet 1997, Fig. 3) effectively display the thermometer calibration and reveal at the same time some of the compositional and underlying crystal-chemical influences. In the present case the ordinate and abscissa values are the mole percentages of $FeTiO_3$ and Fe_2TiO_4 projected to the binaries as detailed earlier.

The modal proportions of Usp-Mt relative to Ilm-Hem increase with decreasing f_{O_2} in our experiments because of Eq. 2 and the mass-balance constraint; as a result Usp-Mt was not present in experiment 6 at ΔNNO ≈ 3.5, and Ilm-Hem was hard to find in experiments below ΔNNO = 0. Average compositions of coexisting FeTi-oxides grown from composition I, after projecting out the components of Al_2O_3, are shown in the Roozeboom plot of Fig. 4. Uncertainty bars are typically larger for Ilm-Hem than for Usp-Mt. Also note that in some cases the desired ten spot analyses of Ilm-Hem could not be obtained because of small crystal size (Tables 3, 4, 5, 6). Al_2O_3 in the Usp-Mt varies from 1.6 to 2.1 wt.% (about 4 mol.% of the hercynite component), and in Ilm-Hem from 0.24 to 0.68 wt.% (i.e., mostly less than 1% of the

corundum component). The average compositions of the FeTi-oxides (Tables 3, 4, 5, 6) define 800 and 900°C isotherms that both contain an inflection. The inflections indicate significant non-ideality in the rhombohedral phase and may be interpreted as primarily reflecting the thermodynamic consequence of long-range order of Fe and Ti in ilm-rich ($R\bar{3}$) compositions and the second-order transition to FeTi-disordered hem-rich ($R\bar{3}c$) compositions (Ghiorso 1990). Accordingly, our isotherms have been hand-drawn to fit the data-points and to reflect a change to vertical slope (i.e., a narrow solvus gap, Ghiorso et al. 2003) near ilm_{60}. In the simple system FeTiO, the transition compositions are 59% ilm at 800°C and 64% ilm at 900°C (Ghiorso 1990; Harrison et al. 2000a; Harrison and Redfern 2001). The small amount of the corundum component in Ilm-Hem in composition I charges seem unlikely to seriously displace the transition curve, but it may have widened the solvus slightly.

In comparison to QUILF (Andersen and Lindsley 1988), our data at 800 and 900°C show a more usp-rich spinel coexisting with Ilm-Hem when ilm > 50% and the converse when ilm < 50% (Fig. 4). These differences result in part from the strongly inflected nature of our isotherms. The QUILF isotherms at these temperatures (Fig. 4) show mild inflections due to the positive regular solution model adopted for the rhombohedral solid solutions by Andersen and Lindsley (1988). These authors recommended that their calibration not be used over most of the range in Ilm-Hem covered in Fig. 4. A comparison of the hc-mt and hc-usp solvi (Ghiorso and Sack 1991) suggests that non-ideal differences would displace our data-points ≈2 mol.% usp down relative to the isotherms for the pure FeTiO system; the presence of Al clearly does not explain the differences in calibrations. We believe that they reflect in part the inclusion in the A&L (and G&S) isotherm-fits of experiments using the Ni–NiO solid oxygen buffer. There is evidence that these experiments may have been influenced by the take-up in the charge of Ni diffusing through the capsule walls (D.H. Lindsley, personal communication). It is significant that experiments in the pure system using the Hed-Adr-Mt-Qtz (HAMQ) buffer at 800 and 890°C (Andersen and Lindsley 1988) agree quite well with our isotherms (Fig. 4).

Our data show a somewhat better fit to isotherms derived from Ghiorso and Sack (1991), who incorporated FeTi order–disorder into their model for ilm-hem solid solutions. The inflections in the isotherms on the Roozeboom plot remain a feature of the system up to 1,300°C (Lattard et al. 2005).

Compositional variability of Ilm-Hem within each run-product, especially in the 800°C series of experiments, tends to be greatest in Ilm-Hem falling within the range 50–80% ilm. This reflects in part the very small free energy differences in intermediate Ilm-Hem solutions. We shall see that this is the case for Ilm-Hem in all four bulk compositions studied.

In a few cases at 800°C (and rarely at 900°C, Fig. 2), oxide compositions are out-of-sequence in terms of ΔNNO with respect to neighboring experiments. We attribute this to failure of the membrane to equilibrate H_2 or to changes in redox state (mostly upwards) during the run. Compositions nevertheless appear to correctly record the experimental temperature.

Bulk composition II (FeTiAlMgO system)

The principal effects of the addition of 1 wt.% MgO to composition I are an increase in the content of aluminate components in Usp-Mt at the expense of ferrite (Fig. 5a, b),

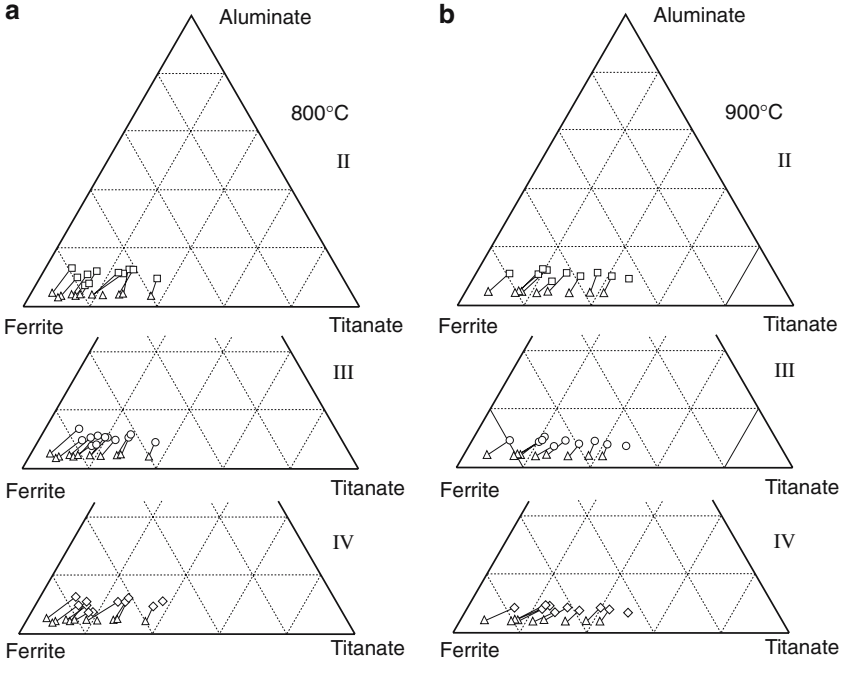

Fig. 5 The composition of FeTi-spinels at 800°C (**a**) and 900°C (**b**) in the ternary diagram ferrite–titanate–aluminate. *Triangles* are composition I spinels, *squares* composition II, *circles* composition III, and *diamonds* composition IV. *Tielines* link products of the same experiment; they are not coexisting pairs

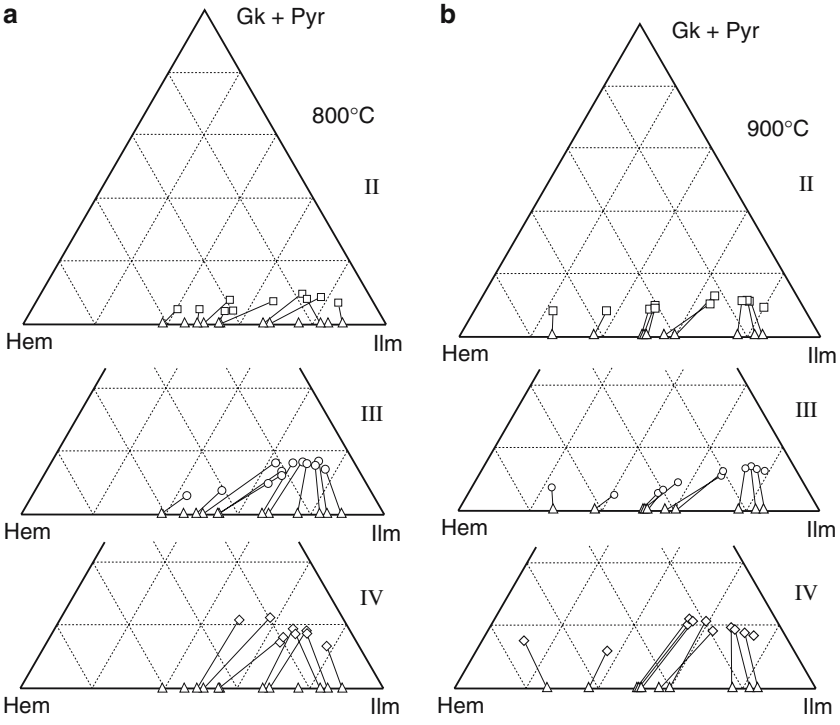

Fig. 6 The composition of rhombohedral oxides at 800°C (**a**) and 900°C (**b**) in the ternary diagram hematite–ilmenite–geikielite + pyrophanite. *Symbols* are the same as in Fig. 5

and the formation of geikielite at the expense of hem in Ilm-Hem (Fig. 6a, b). Projection from the top to the base of the triangles in Figs. 5 and 6 gives the apparent proportions of components in the system FeTiO already shown in Fig. 2. The increase in projected %usp (Fig. 2a) caused by MgO addition is for the most part proportionally larger than that of %ilm (Fig. 2b) for a given T, P, and f_{O_2}. The Roozeboom plot (Fig. 7), by necessity, shows the projected proportions of usp, mt, ilm, and hem. The isotherms are not very different from those for the Mg-free composition I, except when Ilm-Hem compositions are poorer than about 60% ilm. However, the data-points for individual experiments have moved up and to the right along the isotherms, as shown in Fig. 8a, especially for Ilm-Hem in the solvus region, where ΔNNO = 0.7–1.5 (Fig. 2). These shifts can be interpreted as a response to increased non-ideality of gk-hem with respect to ilm-hem, and similarly qan-mt with respect to usp-mt. There seems to be a larger break in slope (solvus?) of the isotherms at about 60–70% ilm (Fig. 7) in comparison to composition I. In this context, it is important to note that the sudden change in slope in projection at 900°C (Fig. 7) is 4–5% ilm lower than it would be if the ≈10% gk were instead included in "ilmenite" on the diagram. The latter procedure might be more appropriate for locating the order–disorder transition and the solvus limits, if geikielite simply proxies for ilmenite in this regard. The same comment applies to the Roozeboom diagrams we use for compositions III and IV.

Figure 7 also shows data-points for FeTi-oxides from similar redox-controlled hydrothermal experiments on glass made from Pinatubo dacite (Scaillet and Evans 1999, here with revised analyses). Comparison with the present results, with comparable amounts on Mg in the FeTi-oxides, is good, especially when allowance is made for the higher Al_2O_3 content of Usp-Mt in the plagioclase-free rhyolite composition. This increase in Al_2O_3 can be expected to have shifted our isotherms slightly to more mt-rich compositions.

It is not clear how much of the increase from 4 to ≈10% of aluminate (Fig. 5a, b) in Usp-Mt relative to composition I corresponds to Mg-spinel or to hercynite. At 800°C the gk content of Ilm-Hem rises from 4 to

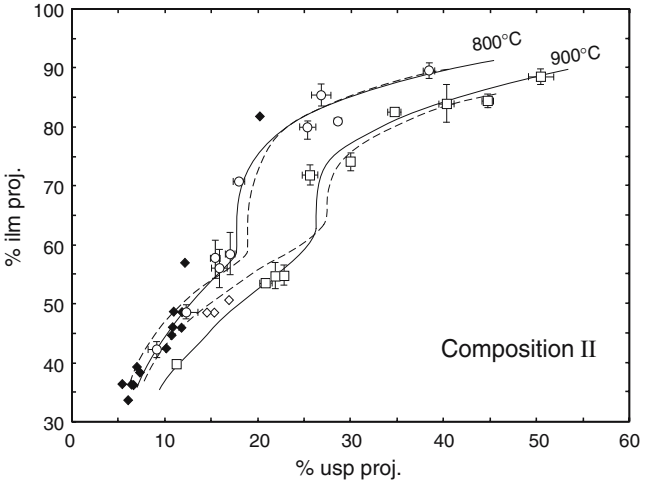

Fig. 7 Roozeboom plot for composition II (system FeTiAlMgO). *Dashed lines* are isotherms from Fig. 4 for composition I. *Continuous isothermal lines* are drawn by hand. Same *symbols* as Fig. 4. Experiments on Pinatubo dacite (Scaillet and Evans 1999): *open diamonds* 834°C and *filled diamonds* 780 ± 5°C

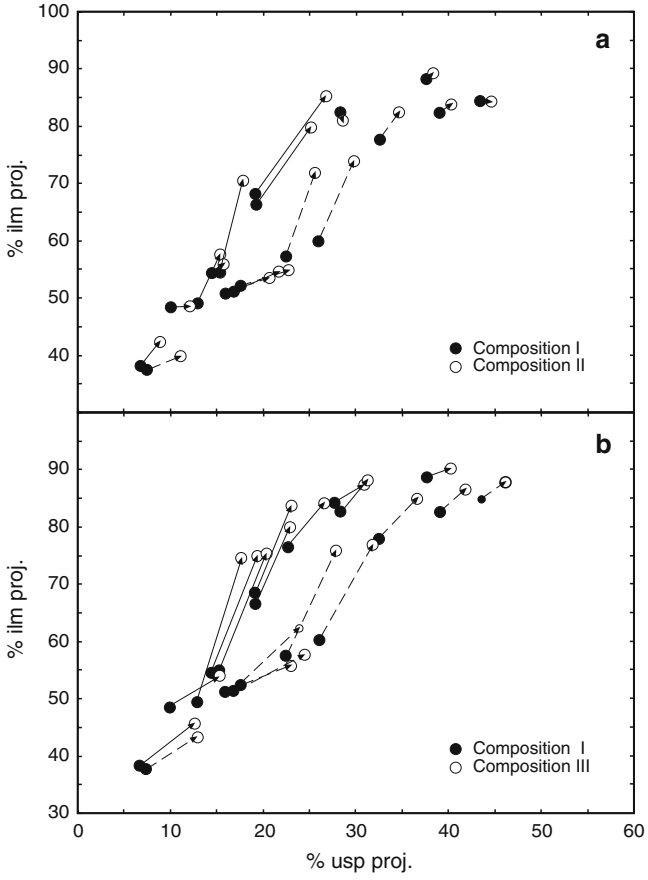

Fig. 8 Comparison of Roozeboom plots at 800 and 900°C between composition I and II (**a**), and between composition I and III (**b**). *Arrows* point from I to II and III in each experiment, respectively

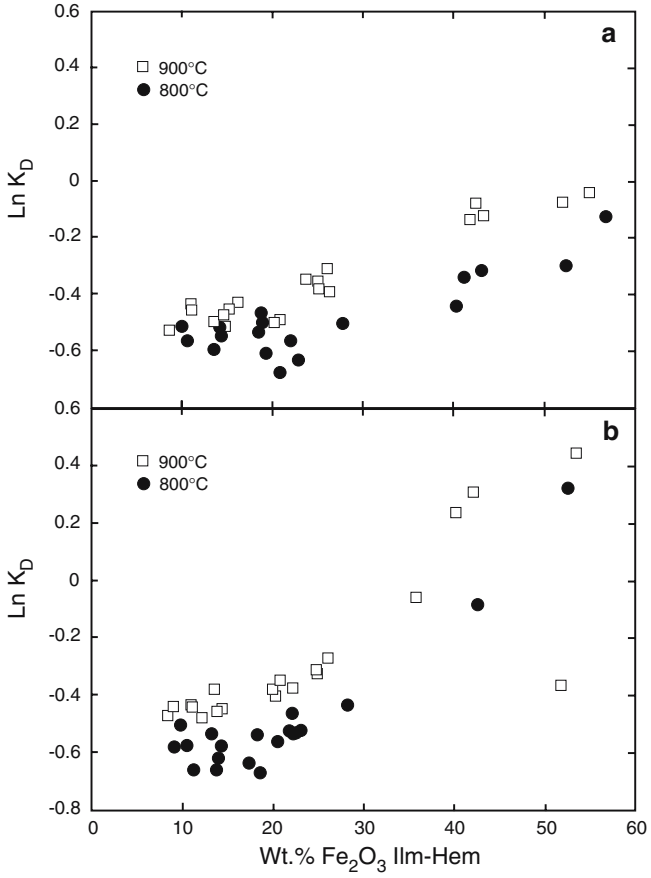

Fig. 9 Ln K_D [K_D = $(Mg/Fe_{Usp\text{-}Mt})/(Mg/Fe_{Ilm\text{-}Hem})$] in compositions II and IV (**a**) and ln K_D [K_D = $(Mn/Fe_{Usp\text{-}Mt})/(Mn/Fe_{Ilm\text{-}Hem})$] in compositions III and IV (**b**), vs. wt.% Fe_2O_3 in Ilm-Hem

9 mol.% toward the ilmenite end of the series (Fig. 6a), and at 900°C the gk component rises from 9 to 12 mol.% (Fig. 6b). Ghiorso and Sack (1991) noted this temperature dependence for natural ilmenites. The composition-dependent uptake of gk in Ilm-Hem would reflect the non-ideality differences mentioned above.

When expressed as the ratio $MgO/Fe^{2+}O$, MgO is enriched in Ilm-Hem over Usp-Mt, but not as strongly as found by Pinckney and Lindsley (1976) in the Al-free system FeTiMgO. The $Fe^{2+}Mg_{-1}$ ion-exchange reaction is:

$$MgFe_2O_4 + FeTiO_3 = Fe_3O_4 + MgTiO_3 \quad (3)$$

The ln K_D of this reaction is less negative at 900 than 800°C (Fig. 9a), in agreement with Lindsley (1991, Fig. 13), but the ln K_D also correlates with the Fe_2O_3 content of the rhombohedral phase, such that the preference is projected to reverse itself when $\%Fe_2O_3 > 60$. This reflects in part the trends seen in Figs. 5 and 6. With Fe^{3+} present in the system, a Fe^{2+}-free equilibrium also holds:

$$Mg_2TiO_4 + Fe_2O_3 = MgFe_2O_4 + MgTiO_3 \quad (4)$$

The existence of this equilibrium is presumably responsible for the trends in Fig. 9a.

The $MgO/Fe^{2+}O$ ratio of Usp-Mt increases with increasing redox state, and correlates well with MgO/FeO in orthopyroxene.

The change from composition I to composition II at constant T, P, and f_{O_2} should of course have no effect on log K of the exchange thermometer reaction 1 or on log K (or $\log f_{O_2}$) of the redox reaction 2. The goal of a subsequent paper (M.S. Ghiorso et al., in preparation) is to calibrate activity–composition models that make this a reality for both reactions. We can see already that some cancellation of compositionally induced shifts occurs because both the ferrite and the hem components are reduced as a result of the addition of MgO.

If we examine the compositional effect on the redox reaction simply in terms of a change in log K_{ideal} (log K of reaction 2 expressed in terms of un-projected mole fractions of hem and mt), we find that cancellation is far from complete. Composition II oxides appear to have formed at as much as 1 log unit of oxygen fugacity lower than those in composition I in the same experiment. For the same reason, log K_{ideal} of the thermometer reaction 1 fails as any sort of suitable proxy for log K.

The high values of aluminate in Usp-Mt may be attributed in part to the contents of Mg (and Mn, see below) in the oxide minerals, but also to the fact that our

rhyolite glass starting material contains no Ca. In natural magmas, Ca would ordinarily complex with Al in the liquid as an "anorthite" component, thus reducing the amount of Al likely to enter the oxide minerals.

Bulk composition III (FeTiAlMnO system)

The compositional shifts caused by the addition of 0.8% MnO are similar in character to those induced by MgO, but somewhat larger, namely: (1) larger increases in projected %ilm and %usp when compared to composition I (Fig. 2), as much as 19% ilm in the range 55–80% ilm and ΔNNO from 0.5 to 1.7 and (2) decreases in mt and hem components throughout, balanced by increases in aluminate in Usp-Mt and pyrophanite in Ilm-Hem (Figs. 5, 6). Aluminates are comparable to the corresponding amounts in composition II. There is more pyrophanite in Ilm-Hem at 800°C than at 900°C, in agreement with the temperature dependence observed in experiments (Mazzullo et al. 1975; Lindsley 1991, Fig. 15) and in natural ilmenites (Ghiorso and Sack 1991).

Noticeable in Fig. 6a, b, composition III, is the variable uptake of pyrophanite in Ilm-Hem: three times as much in ilm-rich compositions as in hem-rich compositions. Since the bulk composition of the charge has a constant content of MnO, the locus of MnO contents in Fig. 6a, b, to a first approximation defines an isopotential line. This suggests that the activity coefficient of pyrophanite in Hem is 3× larger than its value in Ilm. There will be corresponding differences in the activity coefficients of hem and ilm in pyrophanite according to the Gibbs–Duhem equation at fixed P and T. The non-ideal effect of Mn substitution is thus larger than in the case for Mg.

The isotherms for composition III (Fig. 10) appear to be more inflected than for compositions I and II. At low values of ΔNNO, Ilm-Hem is richer in ilm, and at high values of ΔNNO it is poorer in ilm. This suggests more non-ideal behavior of Ilm-Hem, perhaps with a solvus of significant width.

MnO partition between the two oxides (relative to $Fe^{2+}O$) is similar in behavior to MgO, but the dependence of ln K_D on the Fe_2O_3 content of the Ilm-Hem is almost twice as strong, such that ln K_D becomes positive when $\%Fe_2O_3$ is greater than about 40 (Fig. 9b). There is an unmistakable change in slope of the trends in Fig. 9b at 30–40 wt.% Fe_2O_3, and we assume that this reflects passage across the order–disorder transition in Ilm-Hem. Molecular fractions of Fe^{2+} cancel when ln K_D (Mn/Fe^{2+}) is subtracted from ln K_D (Mg/Fe^{2+}): that is, Fig. 9a minus Fig. 9b. This difference corresponds to the y-intercept on the Bacon–Hirschmann diagram (Fig. 3). Because this difference becomes increasingly negative as Fe_2O_3 in Ilm-Hem extends beyond 30%, the B–H correlation is shifted downwards. For experiment 2 the downshift is 0.48/2.303 or 0.2 log units. Thus, for Ilm-Hem in the disordered hem-rich compositional range, the B–H diagram should consist of a series of isopleths for %hem having intercepts more than 0.2 lower than the published correlation. Three pairs from granitic glass recrystallized at ΔNNO = 2.5 show this behavior (Dall'Agnol et al. 1999). Iron–titanium oxide pairs in natural volcanics with hem > ilm are, of course, extremely rare.

Log K_{ideal} of the redox reaction 2 differs from that in composition I by as much as −1 to −2 log units. This means that any thermodynamic formulation of the thermobarometer in complex systems must incorporate sizeable temperature- and composition-dependent activity coefficients when significant amounts of MnO are present.

Bulk composition IV (FeTiAlMgMnO system)

The compositionally induced shifts are even larger when Mg and Mn are added together (Figs. 2, 11, cf. 7

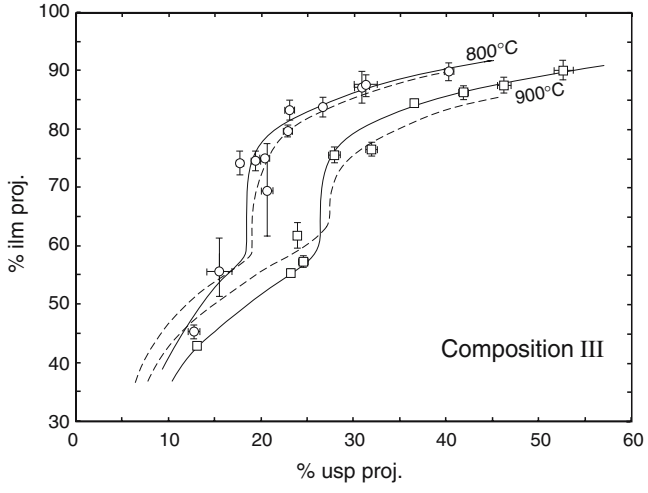

Fig. 10 Roozeboom diagram for composition III (system FeTiAlMnO). Same *symbols* as Fig. 4. *Continuous lines* drawn by hand. *Dashed lines* are our isotherms from Fig. 4

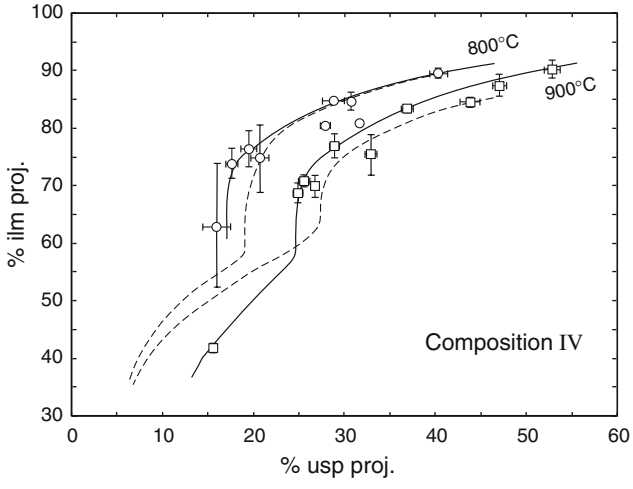

Fig. 11 Roozeboom diagram for composition IV (system FeTiAlMgMnO). Same *symbols* as Fig. 4. *Continuous lines* drawn by hand. *Dashed lines* are our isotherms from Fig. 4

and 10). Ilm-Hem does not cross the solvus/transition region until ΔNNO reaches as high as 2.0 (Fig. 2b).

A Bacon–Hirschmann style plot (not shown here) of log(Mg/Mn) in oxide pairs from all three bulk compositions II, III, and IV shows a straight line extending over three orders of magnitude and possessing a slope of 0.95. This compares with a slope of 0.932 in the regression line of Bacon and Hirschmann (1988). The slope of our line is independent of T and f_{O_2}. It would appear that the substitution of Mg or Mn or both in Ilm-Hem does not obey Henry's Law; a slope greater than unity would have indicated failure of Henry's Law in the Usp-Mt.

Orthopyroxene

At 900°C euhedral acicular crystals of orthopyroxene (Fig. 1c) up to 500 μm × 30 μm in section grew in experiments using compositions II (+MgO) and IV (+MgO and MnO). Orthopyroxene also crystallized at 800°C in composition IV experiments, but its place is taken by biotite in composition II experiments.

Averages of microprobe analyses (Table 7), when recast to a formula containing four cations and six oxygens, suggest that 0.045 ± 0.015 atoms/pfu of Fe^{3+} are present, but the amount of this component shows no detectable dependence on f_{O_2}. Al_2O_3 mostly ranges from 2 to 5 wt.% in the Mg experiments (II) and 1.5 to 3.5% in the Mg + Mn experiments (IV). TiO_2 contents greater than about 0.30 wt.% probably signify tiny inclusions of FeTi-oxides in the analyzed volume.

The ferrosilite content of orthopyroxene ideally should reflect the equilibrium:

$$2Fe_3O_4 + 6SiO_2\,(\text{liquid}) = 6FeSiO_3 + O_2\,(\text{vapor}) \qquad (5)$$

(we might write this with H_2 and H_2O instead of O_2). When early-grown crystal-core compositions are excluded (Fig. 12), the ferrosilite content of orthopyroxene in composition II experiments at 900°C shows the predicted inverse correlation with ΔNNO, declining from 42 ± 3% at ΔNNO = −0.41 to 20 ± 2% at ΔNNO ≈ +2.5. In composition IV experiments, the ferrosilite content expressed as percent Fe/(Fe + Mg + Mn) declines from 45 ± 3 to 19 ± 2% over the same range in ΔNNO. In the context of equilibrium 5, the three log-unit increase in f_{O_2} is the dominant control on the composition of orthopyroxene, only slightly counterbalanced by the 0.25 decrease in log $X_{ferrite}$ in spinel over the same range (Fig. 5). Calculations by Lindsley et al. (1990) and Frost and Lindsley (1992) showed the same trend in X_{Fe} of orthopyroxene in the QUIlOp assemblage, but at slightly higher X_{Fe} than ours, consistent with quartz-saturation.

At 800°C the ferrosilite content of orthopyroxene in composition IV decreases from 50 ± 1% at ΔNNO = −0.27 to 20 ± 2% at ΔNNO ≈ 2.5. Thus, the 800°C isotherm for composition IV is roughly 5–10% ferrosilite above that at 900°C for comparable values of ΔNNO. This observation is again consistent with Lindsley et al. (1990) and relates to the higher activity of SiO_2 in the liquid and larger %ferrite in the spinel in the 800°C as compared to the 900°C experiments (Fig. 5).

Biotite

At 800°C biotite crystals on average 15 μm × 2 μm in cross-section (Fig. 1b) grew in charges of composition II (+MgO). Their iron contents may be expected to reflect the equilibrium:

Table 7 Average compositions (wt.%) of orthopyroxene, composition II, 900°C

Run no.	16	18	19	26	20	13	14	25	21	2
ΔNNO	−0.41	−0.02	0.47	0.73	1.16	1.38	1.59	1.88	1.91	2.5
No. of spots	7	8	10	6	10	8	10	7	6	10
SiO_2	49.39	50.43	50.49	50.71	51.52	51.26	51.29	51.83	51.27	51.26
TiO_2	0.40	0.39	0.40	0.36	0.33	0.32	0.27	0.29	0.28	0.25
Al_2O_3	3.36	3.49	3.86	3.88	4.08	3.20	5.08	4.05	4.72	4.25
FeO	25.61	23.01	21.90	21.43	16.82	18.57	16.23	15.95	15.74	13.12
MgO	20.18	22.55	23.32	22.95	27.18	25.41	27.44	27.27	26.92	28.98
MnO	0.00	0.01	0.05	0.20	0.07	0.22	0.05	0.19	0.18	0.21
K_2O	0.04	0.05	0.04	0.08	0.04	0.02	0.04	0.05	0.07	0.03
Total	98.98	99.91	100.05	99.62	100.05	98.99	100.40	99.63	99.16	98.10
Four cations, six oxygens										
Si	1.878	1.872	1.861	1.879	1.852	1.883	1.831	1.867	1.855	1.850
Ti	0.012	0.011	0.011	0.010	0.009	0.009	0.007	0.008	0.007	0.007
$^{[4]}Al$	0.122	0.128	0.139	0.121	0.148	0.117	0.169	0.133	0.145	0.150
$^{[6]}Al$	0.029	0.025	0.029	0.048	0.025	0.022	0.045	0.039	0.056	0.031
Fe^{3+}	0.037	0.043	0.046	0.030	0.054	0.040	0.057	0.041	0.040	0.055
Fe^{2+}	0.777	0.671	0.629	0.634	0.452	0.531	0.428	0.439	0.436	0.341
Mg	1.144	1.248	1.281	1.267	1.456	1.391	1.460	1.464	1.451	1.559
Mn	0.000	0.000	0.002	0.006	0.002	0.007	0.002	0.006	0.006	0.006
K	0.002	0.002	0.002	0.004	0.002	0.001	0.002	0.002	0.003	0.001
Fe/(Fe+Mg)	0.416	0.364	0.345	0.344	0.258	0.291	0.249	0.247	0.247	0.203
Fe^{3+}/Fe(total)	0.045	0.060	0.068	0.046	0.108	0.070	0.117	0.085	0.084	0.139

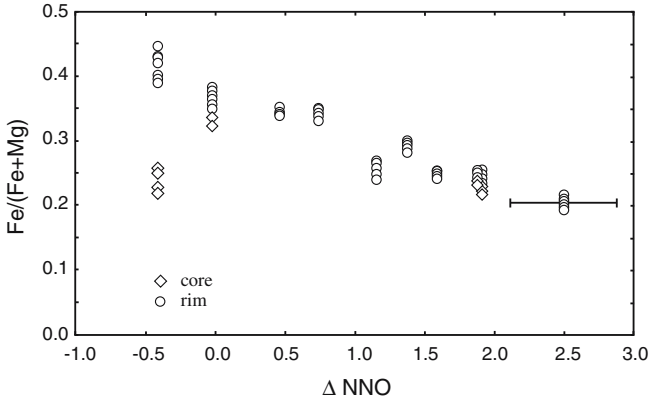

Fig. 12 Fe/(Fe + Mg) of orthopyroxene vs. experimental ΔNNO at 900°C, composition II

$$Fe_3O_4 + KAlSi_3O_8 \text{ (liquid)} = \text{annite} + O_2 \text{ (vapor)} \quad (6)$$

Figure 13 shows that the ratio Fe/(Fe + Mg) of biotite declines from 0.50 at ΔNNO = −0.27 to 0.20 at ΔNNO≈3.5. As for orthopyroxene, the dominant control of biotite composition is the f_{O_2}. Variation in the activity of the orthoclase component of the rhyolite liquid in the different experiments at 800°C is probably small. When corrected for contamination by glass, microprobe analyses of the biotites show between 2.5 and 4.9 wt.% TiO_2, with only a poor correlation with ΔNNO and the Ti contents of the oxide minerals.

Concluding remarks

To provide calibration of the FeTi-oxide thermobarometer at conditions of temperature and oxygen fugacity poorly covered by previous equilibrium experiments, a synthetic, low-melting rhyolite composition containing TiO_2 and iron oxide, with further additions of MgO, MnO, and MgO + MnO, was used in hydrothermal experiments to crystallize Ilm-Hem and Usp-Mt solid solutions at 800 and 900°C under redox conditions slightly below NNO to ≈3 $\log_{10} f_{O_2}$ units above the NNO oxygen buffer. The experiments took advantage of our ability to control and measure f_{O_2} in high P–T hydrothermal experiments in arbitrary steps over a range of redox states encountered in many igneous systems. Crystallization from liquid avoided dependence on lattice diffusion to achieve equilibrium mineral compositions. While equilibrium was not proven in the customary sense by bracketing, the general homogeneity of FeTi-oxide run-products and the systematic relations among their Fe, Ti, Mg, and Mn contents support the attainment of equilibrium states.

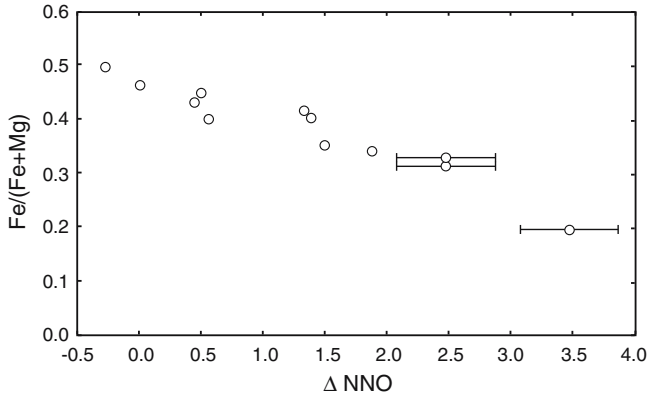

Fig. 13 Fe/(Fe + Mg) in biotite in 800°C experiments on composition II vs. experimental ΔNNO (calculated ΔNNO for experiment 22)

In all four bulk compositions studied, a profound change in the d(ilm%)/d(usp%)-slope of isotherms was found to take place at ≈60% ilm. This is consistent with major control of the FeTi-exchange equilibrium by gradual change in long-range order of Fe and Ti in ilmenite, the presence of the $R\bar{3}$ to $R\bar{3}c$ structural transition, and the likely existence of a solvus at 800 and 900°C. This feature of the system accounts in part for the difference between our results and the thermometer calibration of Andersen and Lindsley (1988) when extended "beyond range." The more complete experimental calibration on the range QFM to NNO + 3 accounts for some of the other differences from previous calibrations.

Usp-Mt and Ilm-Hem in the system FeTiAlO were found to contain, respectively, 4% of aluminate components and less than 1% of the corundum component. In charges containing additional MgO or additional MnO, Usp-Mt crystallized with 7–14% of aluminate components, and Ilm-Hem crystallized with 4–13% geikielite component and 5–17% pyrophanite component, respectively. Relative to the FeTiAlO system, these changes are achieved by depletions in the ferrite components of Usp-Mt, and in the hematite component of Ilm-Hem. The projected contents of ulvöspinel and ilmenite are thus larger than in the simple system FeTiO under the same environmental conditions. The compositional shifts in Ilm-Hem are largest in the compositional range $Ilm_{50–80}$, a near-solvus region where the chemical potentials of the hematite and ilmenite components are nearly independent of composition. Addition of MnO induces larger compositional shifts than addition of similar amounts of MgO. The compositional shifts may be attributed to increased non-ideality along joins from end-members magnetite and hematite to their respective Mg- and Mn-bearing aluminate and titanate components. The depletions in hematite and ferrite (largely magnetite) are far from self-canceling in the context of shifts in the thermometric exchange and redox equilibria when expressed in terms of mole fractions (i.e., ln K_{ideal}); full canceling requires appropriate composition- and temperature-dependent activity coefficients in the thermodynamic formulation. The rhombohedral solvus widens by 10–20% ilm as a result of the presence of Mg and Mn in the system.

Ideally, a revised thermodynamic formulation of the FeTi-oxide thermobarometer should not only reproduce the experimental data within reasonable uncertainty limits, but it should also predict estimates of T and $\log f_{O_2}$ that do not correlate with the amounts of Mg and Mn present. A further stringent test of the thermodynamic formulation in the complex system will be that it also reflects the element partitioning relations depicted in Figs. 3 and 9. While our data suggest temperatures 50°C or more lower and oxygen fugacities a few tenths of log units lower than previous calibrations, more precise thermobarometric estimates await completion of the thermodynamic modeling. The close spacing of isotherms in the high f_{O_2} region will make accurate thermometry more difficult there than elsewhere, but, on the other hand, the barometer should still work well.

Acknowledgments This work was supported by grant EAR-0207475 from the National Science Foundation. We thank A. Feenstra, Potsdam, A.T. Anderson, Chicago, D. Lattard and U. Sauerzapf, Heidelberg, and the US National Museum, Washington DC for donating ilmenite microprobe standards, and A. Tourne for laboratory assistance. V. Kress and D. Lattard kindly provided critical reviews prior to submission, and D.H. Lindsley, P. Robinson, M. Rutherford are thanked for their formal reviews. Our collaborator M.S. Ghiorso gave us much helpful advice.

Appendix: microprobe standards

Figures 14 and 15 show the consistent, small differences for FeO and TiO_2 obtained by microprobe analysis in this study using as standards Elba hematite and synthetic TiO_2 and values from wet chemical analysis and synthesis. The reason for these differences is unknown,

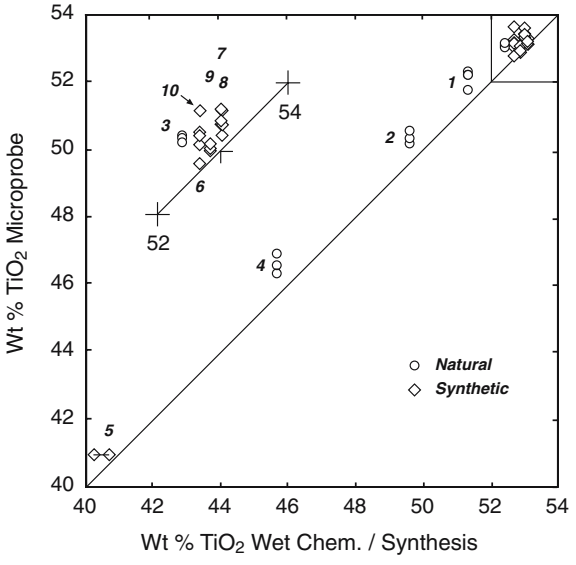

Fig. 14 Microprobe analyses of TiO_2 obtained in repeat sessions compared to wet chemical analyses and assumed synthetic compositions. Sample numbers: *1* Sawyer, *2* A128, *3* K13-134, *4* USNM 96189, *5* 61T60Mx1.5a, *6* FP135, *7* FP97, *8* FP134, *9* FP102, and *10* FP116

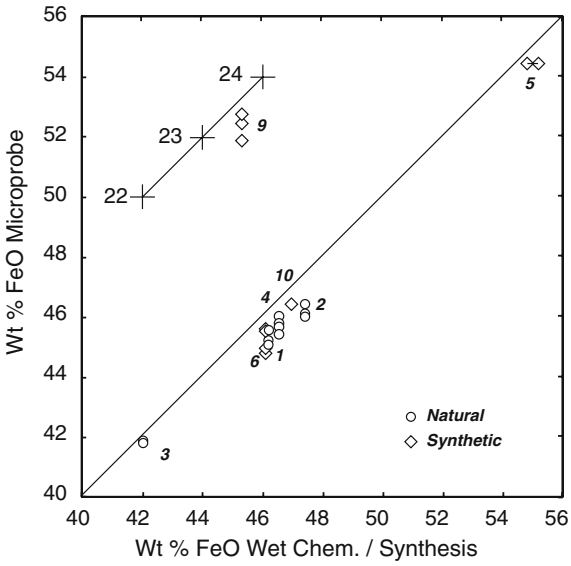

Fig. 15 Microprobe analyses of FeO (total Fe) obtained in repeat sessions compared to wet chemical analyses and assumed synthetic compositions. Sample numbers as in Fig. 14

but it may well relate to the strong characteristic fluorescence of Ti by Fe. Our analytical data (Tables 3, 4, 5, 6) were acquired using the hematite and TiO_2 standards, matrix-corrected with CITZAF, and subsequently corrected, commensurate with Figs. 14 and 15, downwards by 1% relative (TiO_2), and upwards by 0–2% relative (for FeO) in proportion to the TiO_2 content from hematite/magnetite to end-member ilmenite.

Our four analyzed natural ilmenites are A-128 and K13-131.8 from A.T. Anderson, U. Chicago, "Sawyer" from U. California, Berkeley, and USNM 96189 from the Smithsonian Microbeam standard collection. Four synthetic compositions along the join $FeTiO_3$–$MnTiO_3$ were kindly supplied by A. Feenstra, GFZ-Potsdam. They were made in a gas mixing furnace at U. Bern at 900°C and ΔNNO = −5.54 (FP97, $MnTiO_3$, and FP102, $Mn_{0.5}Fe_{0.5}TiO_3$), 950°C and ΔNNO = −5.99 (FP135, $Mn_{0.02}Fe_{0.98}TiO_3$), and 940°C and ΔNNO = −9.72 (FP134, $MnTiO_3$), and were reported to have ideal stoichiometry (no excess Ti) by Feenstra and Peters (1996), based on microprobe analyses and powder XRD. FP97 and FP102 have minor corroded relics of rutile, which could mean that the rhombohedral phase is slightly Ti-depleted. The synthetic FP standards as plotted in Figs. 14 and 15 are assumed to have ideal stoichiometry. Also plotted is our analysis of ferri-ilmenite standard 61T60Mx1.5a supplied by D. Lattard, University of Heidelberg; the composition of this sample is indicated as slightly uncertain owing to the formation of a thin rind of pseudobrookite around its margins. A microprobe analysis by U. Sauerzapf, Heidelberg, of another Bern sample (FP116, 900°C, ΔNNO = −5.54), based on Fe_2O_3 and TiO_2 standards, is also plotted. All the synthetic samples show departure from the 45° line in the same sense as the natural ilmenites.

There seem to be two possibilities: (1) The wet chemical analyses of all four natural ilmenites are slightly in error (TiO_2 too low and FeO too high), and the synthetic ilmenites and pyrophanites have excess Ti; or (2) The analyses of the natural standards are correct, the synthetic samples are stoichiometric, and there is a problem with the microprobe matrix correction.

References

Andersen DJ, Lindsley DH (1979) The olivine–ilmenite thermometer. In: Proceedings of the 10th lunar and planetary science conference, pp 493–507

Andersen DJ, Lindsley DH (1988) Internally consistent solution models for Fe–Mg–Mn–Ti oxides: Fe–Ti oxides. Am Miner 73:714–726

Andersen DJ, Lindsley DH, Davidson PM (1993) QUILF: a Pascal program to assess equilibria among Fe–Mg–Mn–Ti oxides, pyroxenes, olivine and quartz. Comput Geosci 19:1333–1350

Armstrong JT (1988a) Quantitative analysis of silicate and oxide minerals: comparison of Monte Carlo, ZAF and phi-rho-z procedures. In: Newbury DE (ed) Microbeam analysis—1988. San Francisco Press, San Francisco, pp 239–246

Armstrong JT (1988b) Bence–Albee after 20 years: review of the accuracy of alpha-factor correction procedures for oxide and silicate minerals. In: Newbury DE (ed) Microbeam analysis—1988. San Francisco Press, San Francisco, pp 469–476

Bacon CR, Hirschmann MM (1988) Mg/Mn partitioning as a test for equilibrium between coexisting Fe–Ti oxides. Am Miner 73:57–61

Buddington AF, Lindsley DH (1964) Iron–titanium oxide minerals and synthetic equivalents. J Petrol 5:310–357

Dall'Agnol R, Scaillet B, Pichavant M (1999) An experimental study of a lower proterozoic A-type granite from the eastern Amazonian craton, Brazil. J Petrol 40:1673–1698

Evans BW, Scaillet B (1997) The redox state of Pinatubo dacite and the ilmenite–hematite solvus. Am Miner 82:625–629

Feenstra A, Peters T (1996) Experimental determination of activities in $FeTiO_3$–$MnTiO_3$ solid solution by redox reversals. Contrib Miner Petrol 126:109–120

Frost BR, Lindsley DH (1992) Equilibria among Fe–Ti oxides, pyroxenes, olivine, and quartz: part II. Application. Am Miner 77:1004–1020

Ghiorso MS (1990) Thermodynamic properties of hematite–ilmenite–geikielite solid solutions. Contrib Miner Petrol 104:645–667

Ghiorso MS, Sack RO (1991) Fe–Ti oxide geothermometry: thermodynamic formulation and the estimation of intensive variables in silicic magmas. Contrib Miner Petrol 108:485–510

Ghiorso MS, Evans BW, Sauerzapf U, Lattard D, Scaillet B (2003) A new calibration of the Fe–Ti, two-oxide geothermometer and oxygen barometer. Geol Soc Am Abst Programs: 393

Harrison RJ, Redfern SAT (2001) Short- and long-range ordering in the ilmenite–hematite solid solution. Phys Chem Miner 28:399–412

Harrison RJ, Redfern SAT, Smith RI (2000a) In-situ study of the $R\bar{3}$ to $R\bar{3}c$ phase transition in the ilmenite–hematite solid solution using time-of-flight neutron powder diffraction. Am Miner 85:194–205

Harrison RJ, Becker U, Redfern SAT (2000b) Thermodynamics of the $R\bar{3}$ to $R\bar{3}c$ phase transition in the ilmenite–hematite solid solution. Am Miner 85:1694–1705

Holloway JR (1987) Igneous fluids. In: Carmichael ISE, Eugster HP (eds) Thermodynamic modeling of geological materials. Reviews in Mineralogy, vol. 17. Mineralogical Society of America, Washington, pp 211–232

Holtz F, Pichavant M, Barbey P, Johannes W (1992) Effects of H_2O on liquidus phase relations in the haplogranite system at 2 and 5 kbar. Am Miner 77:1223–1241

Lattard D, Sauerzapf U, Käsemann M (2005) New calibration data for the Fe–Ti oxide thermo-oxybarometers from experiments in the Fe–Ti–O system at 1 bar, 1000–1300°C and a large range of oxygen fugacities. Contrib Miner Petrol 149:735–754

Lindsley DH (1962) Investigations in the system FeO–Fe_2O_3–TiO_2. Carnegie Inst Wash Year Book 61:100–106

Lindsley DH (1963) Fe–Ti oxides in rocks as thermometers and oxygen barometers. Carnegie Inst Wash Year Book 62:60–65

Lindsley DH (1991) Experimental studies of oxide minerals. In: Lindsley DH (ed) Oxide minerals: petrological and magnetic significance. Mineral Soc America Rev Mineral 25:69–106

Lindsley DH, Spencer KJ (1982) Fe–Ti oxide geothermometry: reducing analyses of coexisting Ti-Magnetite (Mt) and Ilmenite (Ilm). Trans Am Geophys Union 63:471

Lindsley DH, Frost BR, Andersen DJ, Davidson PM (1990) Fe–Ti oxide-silicate equilibria: assemblages with orthopyroxene. In: Fluid–mineral interactions: a tribute to H.P. Eugster. The Geochemical Society, Special Publication No. 2, San Antonio, pp. 103–119

Mazzullo LJ, Dixon SA, Lindsley DH (1975) T– f_{O_2} relationships in Mn-bearing Fe–Ti oxides. Geol Soc Am Abst Program 7:1192

O'Neill HStC, Pownceby MI (1993) Thermodynamic data from redox reactions at high temperatures 1. An experimental and theoretical assessment of the electrochemical method using stabilized zirconia electrolytes, with revised values for the Fe–"FeO", Co–CoO, Ni–NiO, and Cu–Cu_2O oxygen buffers, and new data for the W–WO_2 buffer. Contrib Miner Petrol 114:296–314

Pattison DRM (1994) Are reversed Fe–Mg exchange and solid solution experiments really reversed? Am Miner 79:938–950

Pichavant M (1987) Effects of B and H_2O on liquidus phase relations in the haplogranite system at 1 kbar. Am Miner 72:1056–1070

Pinckney LR, Lindsley DH (1976) Effects of magnesium on iron–titanium oxides. Geol Soc Am Abst Program 8:1051

Robie RA, Hemingway BS, Fisher JR (1979) Thermodynamic properties of minerals and related substances at 298.15 K and 1 bar (105 Pascals) pressure and at higher temperatures. US Geol Surv Bull:1452

Scaillet B, Evans BW (1999) The 15 June 1991 eruption of Mount Pinatubo I. Phase equilibria and pre-eruption P– T– f_{O_2}– f_{H_2O} conditions of the dacite magma. J Petrol 40:381–411

Scaillet B, Pichavant M, Roux J, Humbert G, Lefèvre A (1992) Improvements of the Shaw membrane technique for measurement and control of f_{H_2} at high temperatures and pressures. Am Miner 77:647–655

Scaillet B, Pichavant M, Roux J (1995) Experimental crystallization of leucogranite magmas. J Petrol 36:663–705

Small JA, Heinrich KFJ, Fiori CE, Myklebust RL, Newbury DE, Dilmore MF (1978) The production and characterization of glass fibers and spheres for microanalysis. Scan Electron Microsc 1:445–454

Spencer KJ, Lindsley DH (1981) A solution model for coexisting iron–titanium oxides. Am Miner 66:1189–1201

Stormer JC (1983) The effects of recalculation on estimates of temperature and oxygen fugacity from analyses of multi-component iron–titanium oxides. Am Miner 68:586–594

Toplis MJ, Carroll MR (1995) An experimental study of the influence of oxygen fugacity on Fe–Ti oxide stability, phase relations, and mineral-melt equilibria in ferro-basaltic systems. J Petrol 36:1137–1170

Venezky DY, Rutherford MJ (1999) Petrology and Fe–Ti oxide re-equilibration of the 1991 Mount Unzen mixed magma. J Volcanol Geotherm Res 89:213–230

Warren PH (1997) The unequal host-phase density effect in electron probe defocused beam analysis: an easily correctable problem. In: Lunar and planetary science conference, abstract, vol XXVIII, p 1497